Basin Research

WILEY

Basin Research IAS EAGE

RESEARCH ARTICLE OPEN ACCESS

Spatiotemporal Growth of Seismic-Scale Syn-Flexural Normal Faults in the German Molasse Basin

Lucas H. J. Eskens[1] | Nevena Andrić-Tomašević[1] | Ajay Kumar[2,3] | Magdalena Scheck-Wenderoth[2,4]

[1]Karlsruhe Institute of Technology, Institute of Applied Geosciences, Karlsruhe, Germany | [2]Faculty of Georesources and Materials Engineering, GFZ German Research Centre for Geosciences, Potsdam, Germany | [3]Department of Earth and Climate, Indian Institute of Science Education and Research Pune, Pune, India | [4]Faculty of Georesources and Materials Engineering, RWTH Aachen University, Aachen, Germany

Correspondence: Lucas H. J. Eskens (lucas.eskens@kit.edu)

Received: 7 March 2024 | **Revised:** 13 December 2024 | **Accepted:** 6 January 2025

Funding: This work was supported by Deutsche Forschungsgemeinschaft.

Keywords: geodynamics | lithospheric strength | Molasse Basin | pro-foreland basin | reflection seismics | syn-flexural normal faults

ABSTRACT

Flexure in pro-foreland basins results from the interplay between (sub)surface loading, foreland plate strength, inherited crustal architecture, and the degree of plate coupling. It is expected that lateral variations in these controlling mechanisms will result in along-strike variations in the flexural profile of the foreland basin. This will directly influence the position and width of the forebulge, thereby altering the associated extensional stress field in space and time around which syn-flexural normal faults accommodate deformation. As such, spatiotemporal variations in the growth of the syn-flexural normal faults in foreland basins may provide valuable information regarding the evolution of an orogen-foreland basin system. However, the relation between syn-flexural normal fault growth and the mechanisms controlling foreland basin flexure remains underexplored. Here, we quantify lateral and vertical throw distributions for growth strata of syn-flexural normal faults in the German Molasse Basin. This allowed us to develop a 4D fault growth model. Our results indicate that the flexure in the German Molasse was associated with both the nucleation of new faults and selective reactivation of pre-flexural faults, with the latter depending on fault burial depth at the onset of flexure. Furthermore, our results suggest that localisation of the extensional strain and deformation at the top of the European plate during flexure controlled the nucleation site of the syn-flexural normal faults in the German Molasse. Additionally, the spatiotemporal variation in the onset of syn-flexural normal fault activity suggests a northward migration rate of 7.8 mm/year of the orogen-foreland basin system. This is consistent with previous estimates based on other independent methods. Lastly, a west-to-east increase in cumulative syn-flexural offsets down-dip the normal faults in the German Molasse Basin may have been controlled by orogen-parallel lithospheric strength variations in the downgoing European plate.

1 | Introduction

Normal faults in rifts (Bosworth 1985; Scholz and Contreras 1998), pro/retro-foreland basins (Bergerat 1987; Bradley and Kidd 1991), and pull-apart basins (Mann et al. 1983; Hempton and Dunne 1984) develop in response to crustal extension. Quantifying their activity in time and space is crucial for reconstructing basin evolution (e.g., Jackson and Rotevatn 2013; Pan et al. 2022). Furthermore, it allows for assessing the effect of geodynamic processes and tectonic inheritance on basin development (e.g., slab rollback, Giba, Nicol, and Walsh 2010; Ring et al. 2010). The growth of normal faults in rift basins has been well-established by quantitative studies (e.g., Gawthorpe et al. 2003; Walsh et al. 2003; Jackson et al. 2017). However, their counterparts in pro-foreland basins, hereafter referred to as foreland basins, have received little attention.

Summary

- The depth-dependent distribution of extensional strain promotes top-down growth of syn-flexural normal faults.
- In the Molasse Basin, faults follow the hybrid, constant-length, and isolated lateral growth models.
- Reactivation of pre-existing faults in the Molasse Basin depends on their burial depth at the onset of flexure.
- A forebulge migration rate of 7.8 mm/year was derived from time–space variations in syn-flexural fault nucleation.
- Basin-parallel variations in foreland plate strength influenced syn-flexural fault growth in the Molasse Basin.

The flexural profile of a foreland basin depends on the interplay between (sub)surface gravitational loading (Flemings and Jordan 1990; DeCelles and Giles 1996; Sinclair 1997a), foreland plate strength (Beaumont 1981; Waschbusch and Royden 1992; Burov 2010), the degree of coupling between the converging plates (Ziegler, Bertotti, and Cloetingh 2002; Willingshofer and Sokoutis 2009), and the inherited architecture of the subsiding crust (structures localising and altering the local stress and strain distribution; Lemcke 1988; Andeweg and Cloetingh 1998). The width of the forebulge (flexural uplift migrating in front of an advancing mountain range; DeCelles and Giles 1996; Roure 2008) depends on the amplitude and wavelength of the flexural profile. For example, a narrow forebulge corresponds to a high amplitude and short wavelength flexural profile (Beaumont 1981; Fosdick, Graham, and Hilley 2014). This directly affects the width of the extensional deformation field around the hinge line of the forebulge, where syn-flexural normal faults accommodate strain (Bradley and Kidd 1991; Supak, Bohnenstiehl, and Buck 2006; Langhi, Ciftci, and Borel 2011). Furthermore, the forebulge and associated extensional strain will migrate cratonward as the mountain range encroaches onto the foreland plate (e.g., DeCelles 2012). As a result, the zone of active syn-flexural normal faulting migrates in both time and space. The examples above illustrate how spatiotemporal syn-flexural normal fault evolution can provide insight into the geodynamic processes that controlled the evolution of an orogenic wedge-foreland basin system.

Previous quantitative assessments of syn-flexural normal fault throw distributions in foreland basins indicate that these structures can nucleate newly at shallow levels in previously unruptured crust and basin fill (Supak, Bohnenstiehl, and Buck 2006; von Hartmann, Tanner, and Schumacher 2016). Alternatively, pre-flexural faults may be reactivated (Bry et al. 2004; Langhi, Ciftci, and Borel 2011). However, the locus of nucleation is primarily controlled by the distribution of extensional strain in the foreland plate (Bradley and Kidd 1991; von Hartmann, Tanner, and Schumacher 2016; Shipilin et al. 2020). Furthermore, it has been shown that syn-flexural faults propagate both up- and downward when active, with vertical growth potentially being inhibited by ductile interbedded stratigraphy (Langhi, Ciftci, and Borel 2011; von Hartmann, Tanner, and Schumacher 2016; Shipilin et al. 2020). Finally, it has been demonstrated that lateral fault growth of newly nucleated syn-flexural faults follows the isolated fault growth model (Cartwright, Mansfield, and Trudgill 1996; Supak, Bohnenstiehl, and Buck 2006; La Bruna et al. 2018).

On the basin scale, previous studies revealed along-strike variations in fault offsets and penetration depth, attributed to the along-strike variations in (1) pre-flexural foreland plate crustal architecture (Bry et al. 2004) or (2) the magnitude of foreland plate deflection (Eskens et al. 2024). Such along-strike variations in growth styles of syn-flexural normal faults in foreland basins hint at orogen-parallel variations in the mechanisms controlling flexure of the foreland plate. Therefore, information distilled from syn-flexural normal fault growth can be inverted to better understand the geodynamic evolution of a foreland basin-orogen system.

In this contribution, we study the syn-flexural normal faults in the German Molasse Basin (Figure 1). This basin developed due to late Eocene to early Miocene Alpine (sub)surface loading, causing flexural subsidence of the European foreland plate (Schmid et al. 1996; Handy et al. 2010). Flexural bending was accompanied by the development of syn-flexural normal faults on the basinward slope of the forebulge (e.g., Lemcke 1988; Bachmann and Müller 1991; Shipilin et al. 2020), hereafter referred to as the distal basin margin. In this study, we quantify throw values of syn-flexural seismic horizons along-strike and down-dip syn-flexural normal faults in two 3D seismic volumes on the distal margin of the German Molasse (which is unaffected by Alpine thrusting; see Figure 1 for locations). This quantitative assessment allows us to evaluate the growth styles and interactions of these faults in 4D. We then compare basin-parallel variations in cumulative syn-flexural throw with (1) crustal/lithospheric strength models for the European plate of previous authors (Spooner et al. 2022), (2) the inherited crustal architecture of the European plate, and (3) the geodynamic evolution of the Alps. This allows us to develop an understanding regarding the link between syn-flexural normal fault growth in the Molasse Basin and the mechanisms that governed flexural subsidence of the European plate.

2 | Geological Setting

The German Molasse is part of the Northern Alpine Foreland Basin (Figure 1; Lemcke 1988; Kuhlemann and Kempf 2002). It is subdivided into the Western and Eastern German Molasse based on different tectonostratigraphic evolution (west and east of Munich, respectively; Eskens et al. 2024 and references therein; Figure 1). The Western German Molasse lies north of the Central Alps (defined as the Alps between the Simplon and Brenner Faults; Figure 1) and the Eastern German Molasse lies north of the Eastern Alps (defined as the Alps between the Brenner and Katschberg Faults; Figure 1). The basin developed from the late Eocene to early Miocene due to the flexural subsidence of the European plate. This flexure was induced by Alpine slab and topographic loading (Eskens et al. 2024 and references therein) and sedimentary loading of the basin fill. This flexural subsidence was accompanied by the growth of normal

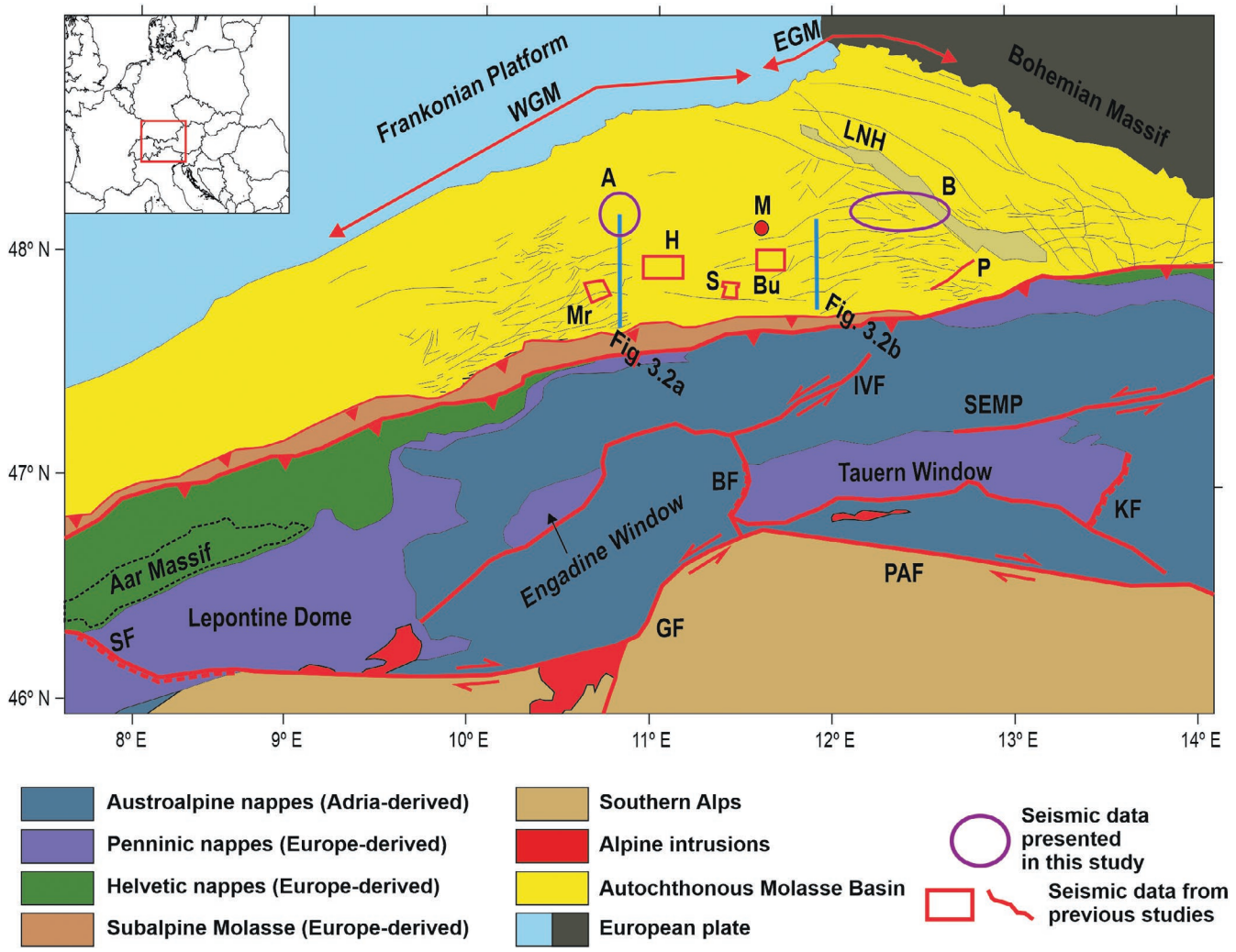

FIGURE 1 | Map of the major tectonic units in the Alps and the European foreland. Modified from Schmid et al. (2004). Thin black lines in the Molasse Basin indicate the locations of syn-flexural normal faults, based on the GeoMol project, as well as data from previous studies (Mraz et al. 2018; Freudenberger and Schwerd 1996). (A) Seismic volume A and (B) seismic volume B presented in this study. BF, Brenner Fault; GF, Giudicarie Fault; IVF, Inntal Valley Fault; KF, Katschberg Fault; LNH, Landshut-Neuoetting High; PAF, Periadriatic Fault; SF, Simplon Fault; SEMP, Salzach-Ennstal-Mariazell-Puchberg Fault; WGM, Western German Molasse; EGM, Eastern German Molasse. Locations of seismic data presented in previous studies: Bu = Budach et al. (2018), H = von Hartmann, Tanner, and Schumacher (2016), Mr = Mraz et al. (2018), P = Cordero Peña (2007), S = Shipilin et al. (2020).

faults striking subparallel to the orogenic front (Lemcke 1988; Ziegler 1990; Bachmann and Müller 1991).

2.1 | The Alpine Hinterland

The flexural subsidence of the German Molasse is inherently related to the Alpine orogeny. Therefore, we provide a synoptic overview of the Alpine tectonics. For a more detailed description, the reader is referred to other contributions (e.g., Schmid et al. 1996; Handy et al. 2010; Le Breton et al. 2021).

The Alps are a stack of Adria-derived Austroalpine and Europe-derived Penninic and Helvetic nappes (Figure 1), recording the closure of the Penninic domain and the subsequent continental collision between the European and Adriatic plates (Trümpy 1960; Schmid et al. 1996; Ziegler et al. 1996). The Penninic domain that separated the European and Adriatic plates consisted of the Piemont-Liguria Ocean, the continental Briançonnais terrane, and the Valais Through (Trümpy 1960; Schmid et al. 1996; Handy et al. 2010; Mohn et al. 2014). Subduction and nappe stacking of the Penninic units below the Austroalpine nappes started in the late Cretaceous (Stampfli et al. 1998; Handy et al. 2010). By the late Eocene, the Penninic domain had been closed, followed by the onset of continental collision and the incorporation of the Helvetic domain into the wedge (Pfiffner 1993; Schmid et al. 1996; Ziegler et al. 1996). Subsequent early Oligocene oceanic slab breakoff led to the exhumation of the previously subducted nappe stack (Davies and von Blanckenburg 1995; Schmid et al. 1996). Continued convergence resulted in folding and southward backthrusting against the Periadriatic Fault of the exhumed nappe stack in the Western and Central Alps (Hurford 1986; Schmid et al. 1996; Schlunegger and Willett 1999; Rosenberg and Kissling 2013). This was translated into the uplift of the orogenic core and external massifs (e.g., Aar Massif, Lepontine Dome and Engadine

Window), due to which the Central Alpine topography reached over 2 km in the Oligocene (Frisch et al. 2001; Kuhlemann 2007) and more than 4 km by the Middle Miocene (Krsnik et al. 2021). In contrast, Oligocene topographies in the Eastern Alps remained low. Their topographic growth started only during the early Miocene, following the continued exhumation of the Tauern Window due to Adriatic indentation (Kuhlemann 2007; Scharf et al. 2013; Schmid et al. 2013; Favaro et al. 2015).

2.2 | Basement and Stratigraphy of the German Molasse

2.2.1 | The Palaeozoic to Mesozoic Basement

The Variscan crystalline basement of the German Molasse is made up of Variscan gneisses and granites, locally cut by fault-bounded Permo-Carboniferous grabens with a clastic fill (Bachmann and Müller 1991). The overlying Middle Triassic to late Cretaceous carbonates and clastics define the Mesozoic passive margin sequence (Meyer and Schmidt-Kaler 1990a; Bachmann and Müller 1991). In the Western German Molasse, the Upper Jurassic stratigraphy subcropping the foreland unconformity is locally heavily karstified (Lemcke 1988; Meyer and Schmidt-Kaler 1990b; Wolpert et al. 2022). This karstification was likely coeval with the erosion of the uplifted Mesozoic passive margin sediments before the onset of flexure (Lemcke 1987). Erosion due to the forebulge passing the former passive margin led to the development of the foreland unconformity, which now separates the Mesozoic passive margin sequence from the late Eocene to early Miocene syn-flexural fill (Crampton and Allen 1995; Ziegler, Bertotti, and Cloetingh 2002).

The European Mesozoic passive margin was characterised by horst-and-graben domains at the future Western German and Eastern German Molasse, respectively (Rhenish Shield and Wasserburger Trog, Lemcke 1988; Eskens et al. 2024). To the north, the Wasserburger Trog and the Palaeozoic to Triassic Giftthal Through in the Eastern German Molasse were delimited by the Lanshut-Neuötting High (Bachmann and Müller 1991; Brink et al. 1992). This was a NW-SE striking intrabasinal high presently oriented obliquely to the orogenic front (Figure 1). Further east, the Austrian part of the Molasse Basin was delimited to the north by the rigid Bohemian Massif (Figure 1). In contrast, such rheological variations did not exist in the European plate in the Western German Molasse.

2.2.2 | The Cenozoic Syn-Flexural Basin Fill

The onset of flexure is recorded by late Eocene neritic to littoral limestones and sands onlapping to the NNW onto the eroded Mesozoic basement in the Eastern German Molasse (Lithothamnium Limestones and Basal Sands; Sissingh 1997; Zweigel, Aigner, and Luterbacher 1998). Subsequent early Oligocene bathyal deposition records a rapid deepening (Rupelian Sands and Marls, Jin et al. 1995; Sissingh 1997; Zweigel, Aigner, and Luterbacher 1998). However, during the late Oligocene to early Miocene, shallowing led to a transition towards littoral and terrestrial conditions in the Western German Molasse (Baustein Beds, Cyrena Beds and Upper Freshwater Molasse; Diem 1986; Kuhlemann and Kempf 2002; Eskens et al. 2024). Littoral to neritic conditions remained dominant in the Eastern German Molasse during the same time (Lower Chattian Marls, Chattian Sands, Upper Chattian Marls and Aquitanian Series; Jin et al. 1995; Zweigel, Aigner, and Luterbacher 1998; Eskens et al. 2024). At the Aquitanian–Burdigalian transition (early Miocene), flooding of the entire German Molasse resulted in the re-establishment of neritic-to-bathyal conditions (Upper Marine Molasse, Baltringer Formation [Fm.] and Hall Fm.; Jin et al. 1995; Zweigel, Aigner, and Luterbacher 1998; Heimann et al. 2009; Heckeberg et al. 2010; Hülscher et al. 2019; Eskens et al. 2024). However, these renewed neritic to bathyal conditions were short-lived, with terrestrial conditions dominating the entire German Molasse since the late Burdigalian (Matter 1980).

2.3 | The Structural Development of the German Molasse

Flexural subsidence of the European foreland plate was accompanied by the development of syn-flexural normal faults generally striking subparallel to the E-W–oriented orogenic front (Figure 1; Lemcke 1988; Bachmann and Müller 1991). These faults developed around the forebulge where extensional stress and strain localised (Supak, Bohnenstiehl, and Buck 2006; Langhi, Ciftci, and Borel 2011). The synthetic faults dip to the south, and the antithetic faults to the north (von Hartmann, Tanner, and Schumacher 2016; Shipilin et al. 2020; Eskens et al. 2024). During ongoing flexure, the number of active faults decreased over time (Eskens et al. 2024).

The development of syn-flexural normal faults in the autochthonous German Molasse (meaning the Molasse Basin unaffected by Alpine thrusting and presently located north of the Alpine Front; Figure 1) started in the late Eocene and Rupelian (Budach et al. 2018; Mraz et al. 2018; Shipilin et al. 2020). Early fault growth was characterised by either reactivation of pre-flexural Jurassic/Cretaceous normal faults (Budach et al. 2018; Mraz et al. 2018) or nucleation of new faults within the Mesozoic sequence or crystalline basement (Shipilin et al. 2020). Rupelian fault activity is only recorded in the basin axis of the Western German Molasse (von Hartmann, Tanner, and Schumacher 2016; Mraz et al. 2018). However, Rupelian syn-flexural normal faults also developed on the distal margin of the Eastern German Molasse (Budach et al. 2018; Shipilin et al. 2020; Eskens et al. 2024). Intra-Rupelian upward termination in the basin axis of the Eastern German Molasse (Figure 2b; Budach et al. 2018; Shipilin et al. 2020) suggests a cessation of fault growth. In the axis of the Western German Molasse, normal faults remained active (Figure 2a; Mraz et al. 2018).

During the Chattian, fault activity continued in the axial Western German Molasse alongside the nucleation of new faults (von Hartmann, Tanner, and Schumacher 2016; Mraz et al. 2018). Contemporaneously, new faults nucleated on the distal margin as well (Eskens et al. 2024). In the axial part of the Eastern German Molasse, new faults also nucleated during the early Chattian within the basin fill (Budach et al. 2018; Shipilin et al. 2020). However, the growth of these newly nucleated faults close to the thrust front quickly ceased (Shipilin et al. 2020). As a

result, these faults did not propagate into the basement, connect with lower segments or grow upward into shallower successions (Shipilin et al. 2020). This resulted in vertically unlinked faults (Figure 2b). Furthermore, Chattian propagation of the Alpine wedge led to the continued incorporation of internal foreland deposits into the Alpine wedge, resulting in the formation of the Subalpine Molasse (Ortner et al. 2015, 2023).

During the Aquitanian, syn-flexural normal faults in the axial Western German Molasse and the distal margin thereof remained active (von Hartmann, Tanner, and Schumacher 2016; Mraz et al. 2018; Eskens et al. 2024). In the Eastern German Molasse, contemporaneous fault activity is only recorded on the distal margin (Eskens et al. 2024). This pattern remained the same during the early Burdigalian, with all faults in the German Molasse being

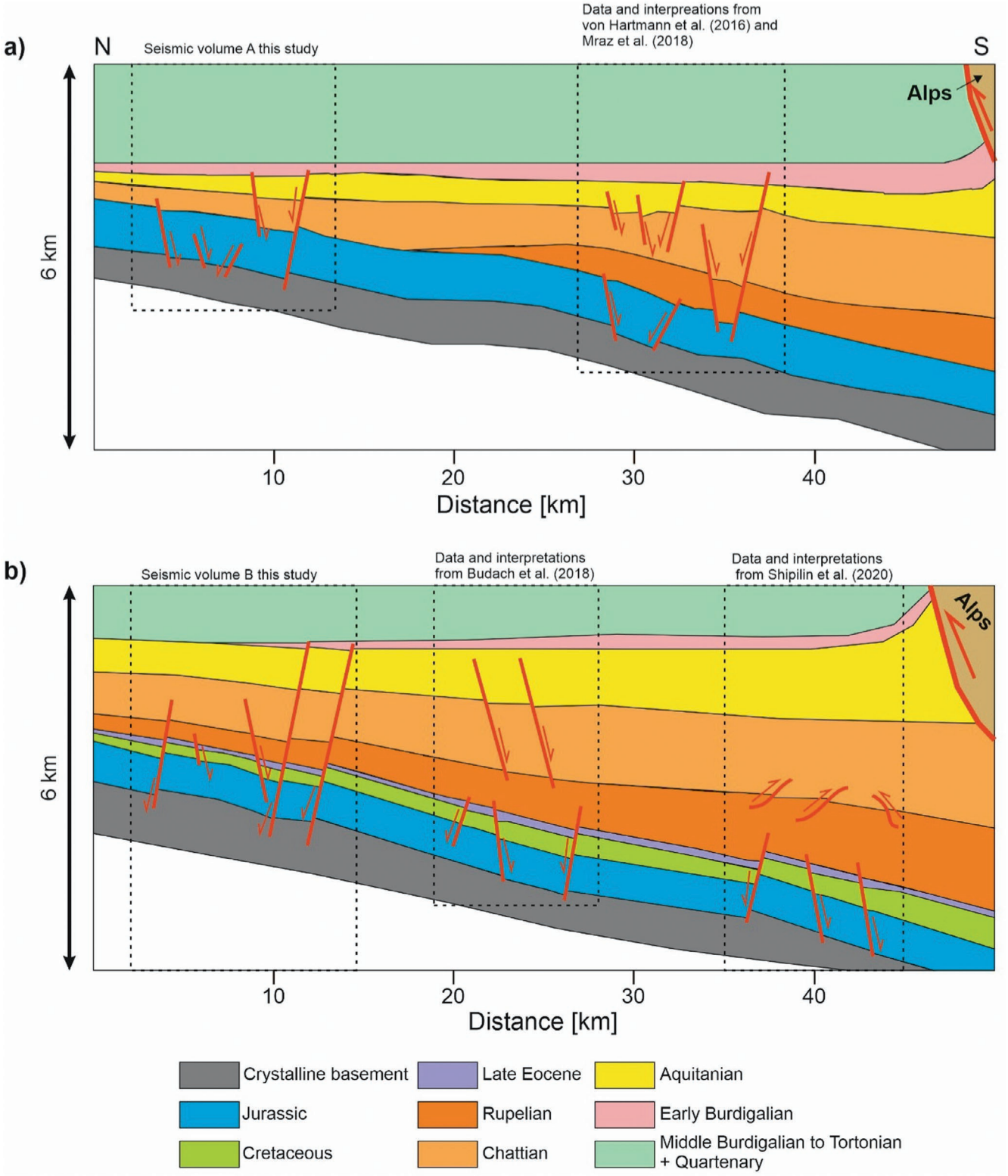

FIGURE 2 | Legend on next page.

FIGURE 2 | Schematic profile of different styles of syn-flexural normal and reverse faults observed in the German Molasse Basin. For locations of these transects, see Figure 1. Faults are only drawn where data are available. (a) In the Western German Molasse, syn-flexural normal faults close to the thrust front are observed to cut the entire Cenozoic syn-flexural fill and the underlying basement (e.g., Mauerstetten fault; Mraz et al. 2018). Furthermore, vertically disconnected sets of faults also exist. Whereas the lower set of faults cuts the basement and terminates within the lower Rupelian stratigraphy, the upper set is restricted to Chattian to early Burdigalian basin fill. On the northern basin margin, syn-flexural normal faults cut the Mesozoic basement, either terminating upward within or cutting the entire syn-flexural fill. The thickness of stratigraphy is only constrained where seismic data are available and interpolated between the volumes. The northern pinch-out of Rupelian stratigraphy is, therefore, not exact. Modified from von Hartmann, Tanner, and Schumacher (2016). (b) In the Eastern German Molasse Basin, closest to the thrust front, a lower set of normal faults cuts the basement and the syn-flexural succession up to the lower part of the Rupelian stratigraphy. In contrast, the upper set of faults is characterised by reverse faults restricted to the upper Rupelian and lower Chattian stratigraphy. Further northward, the same set of lower faults, restricted to the basement and the lower Rupelian stratigraphy, are observed. However, the upper set of faults is characterised by normal faults confined to upper Rupelian to Aquitanian stratigraphy. On the northern basin margin, the syn-flexural normal faults cut the basement, either terminating within or cutting the entire syn-flexural fill. Modified from Wolpert et al. (2022).

sealed by middle Burdigalian stratigraphy (von Hartmann, Tanner, and Schumacher 2016; Mraz et al. 2018; Shipilin et al. 2020; Eskens et al. 2024). Subsequently, syn-flexural faults that had nucleated close to the present-day thrust front during the Chattian in the Eastern German Molasse were reactivated as reverse faults during the middle Miocene (Figure 2b; Shipilin et al. 2020). Contemporaneously, frontal propagation of the Alps largely ceased, with contractional deformation being largely accommodated within the Subalpine Molasse and stationary Alpine wedge (Hinsch 2013; Ortner et al. 2015, 2023; Rosenberg et al. 2018).

3 | Data, Methods and Limitations

This work builds on the detailed seismic-stratigraphic analysis and fault interpretations made in seismic volumes A and B (for locations, see Figure 1) as presented in Eskens et al. (2024). A description of this seismic data can be found in Section A1. Following the seismic interpretations, we quantify throw distributions along-strike and down-dip the syn-flexural normal faults for different reflectors. This allows us to investigate fault growth styles in both time and space (Section 3.1). An analysis of the effect of mechanical stratigraphy on the fault growth styles is presented in Supporting Information S1.

3.1 | Quantitative Fault Kinematic Analysis

In this study, we use the seismic interpretations from Eskens et al. (2024), using the same seismic-stratigraphy (Figure 3), to conduct a detailed kinematic analysis of the syn-flexural normal fault growth styles in the German Molasse. We present results for the two faults with the highest length and syn-flexural throw values in the respective seismic volumes. Because these faults accommodated most of the extensional deformation in the respective seismic volumes, we assume that they represent the structural growth style best. Results for smaller syn-flexural normal faults interpreted in these volumes, which indicate similar growth styles to those presented in the main text, can be found in Figures A4 and A5.

To study the kinematic evolution of the faults, the interpreted seismic horizons and faults are used to generate a structural model in Petrel. Smoothing was applied to the structural model to exclude effects from fault drag. Subsequently, using the 'throw profile' operation for the structural model faults, we can extract the individual throw values for the various reflectors along the fault plane. In this analysis, the throw is defined as the vertical distance between the intersection of a seismic horizon with the fault in the footwall and the hanging wall, respectively. With this approach, the extracted fault throw is a cumulative of dip- and oblique-slip contributions.

First, we apply the 'original' backstripping method (Chapman and Meneilly 1991; Petersen, Clausen, and Korstgård 1992) to the extracted throw profiles for each interpreted stratigraphic horizon. In this method, the throw value of a shallow reflector is subtracted from that of a deeper reflector at the same along-strike position of a fault. The resulting value then represents the syn-kinematic thickening of the stratigraphic unit. Doing this along the fault plane will give a backstripped throw-length (T-x) profile that measures the transient fault activity along its length (e.g., Jackson et al. 2017; Pan et al. 2022). Therefore, we can use this type of profile to determine whether the interpreted normal faults grew according to the isolated, constant length or hybrid fault growth models (Figure A1). We choose this method over the 'modified' backstripping method (Rowan et al. 1998) because this approach implicitly makes the a priori assumption of faults grow according to the isolated fault growth model. Negative values obtained from backstripping are set to zero, as these values indicate a net inactivity of the normal fault.

Second, we constructed 10 throw-depth (T-z) profiles along the length of each T-x profile to provide insight into the stratigraphic position of nucleation and subsequent vertical growth of faults (Figure A2). In these profiles, the stratigraphic level of nucleation is recorded by the reflector with the highest throw value (referred to as throw maximum). The subsequent downward and/or upward growth is then constrained by decreasing throw values for both deeper and shallower reflectors, respectively. These derivations of fault growth based on T-z profiles assume that when a fault accommodates extensional strain, it is active along its entire down-dip length. Lastly, we calculated each seismic-stratigraphic unit's expansion index (EI) at the T-z profile locations. The EI index is a measure of time and magnitude of the across-fault thickening of growth strata when the fault is breaking the free surface. It is calculated by dividing the thickness of a seismic-stratigraphic unit in the hanging wall by the thickness of that same unit in the footwall (Thorsen 1963; Jackson and Rotevatn 2013; Jackson et al. 2017). An EI value of 1 implies that fault activity did not cause across-fault thickening of the stratigraphic unit. In contrast, an EI >1

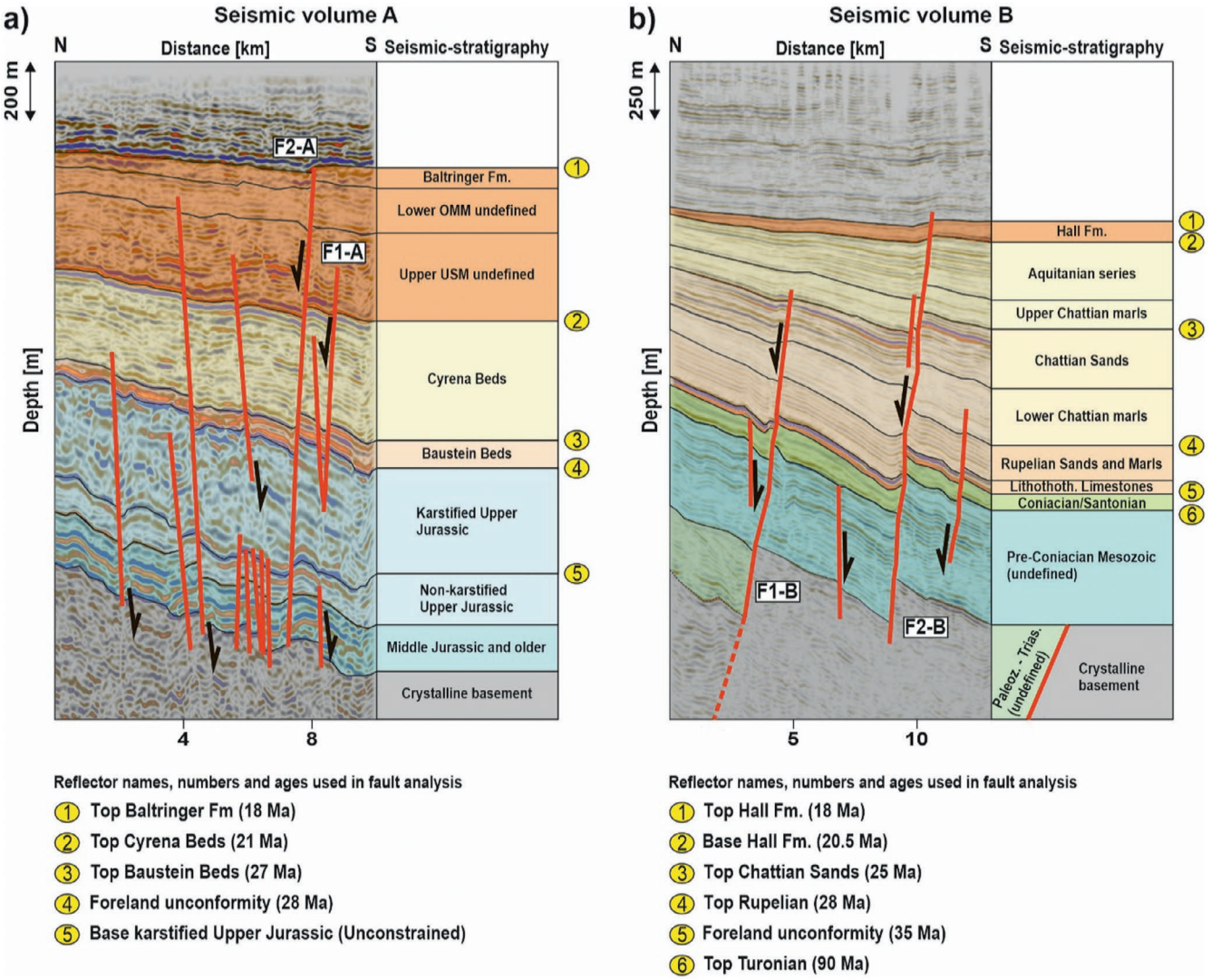

FIGURE 3 | (a) Seismic stratigraphy in seismic volume A, west of Munich, based on Eskens et al. (2024). The ages of reflectors are based on Kuhlemann and Kempf (2002), von Doppler et al. (2005), Heimann et al. (2009), Heckeberg et al. (2010) and Shipilin et al. (2020). Unconstrained means the age of the reflector is unknown, and the unlabelled reflectors are not included in the fault analysis due to poor traceability in the entire seismic volume. Reflector numbers are the same as in Figure 5. OMM, Obere Meeresmolasse; USM, Untere Süßwassermolasse. (b) Seismic stratigraphy in seismic volume B, east of Munich, based on Eskens et al. (2024). The ages of the different reflectors are based on Jin et al. (1995) and Zweigel, Aigner, and Luterbacher (1998). Unconstrained means the exact age of the reflector is unknown, and the unlabelled reflectors are not included in the fault analysis. Reflector numbers are the same as in Figures 6 and 7.

suggests across-fault thickening, that is, syn-kinematic deposition. An EI of <1 is unusual, typically implying difficulties in correctly assessing the thickness of a seismic-stratigraphic unit on either side of the fault (Thorsen 1963; Jackson et al. 2017).

4 | Results

The fault networks in both seismic volumes are dominated by E-W and NW-SE striking faults (Figure 4). Most of the faults strike E-W, with NW-SE striking faults characterising relay faults (e.g., F5-B in Figure 4d). The exception to this is F1-B, which is the upward extension of the basin-bounding fault of the Palaeozoic-Triassic Giftthal Through (Figure 4d; Bachmann and Müller 1991; Eskens et al. 2024). Apart from syn-flexural normal faults, the variance attribute of the foreland unconformity reflector in seismic volume A also reveals elongated, meandering features (Figure 4a,b). These are interpreted as a drainage network of the karstified Upper Jurassic sequence (Lemcke 1987; Eskens et al. 2024; Figure 4a,b). Furthermore, circular shapes with high variance values delineate sinkholes (Figure 4a). The syn-flexural fault locations do not show a spatial relation with these karst features (Figure 4a,b).

4.1 | Quantitative Assessment of Throw Distributions of the Syn-Flexural Normal Faults

4.1.1 | Syn-Flexural Normal Faults Growing According to the Isolated Model

Early Chattian fault patches along the entire length of faults F1-A and F2-A were initially laterally disconnected (T-x profiles in Figure 5a,b). Subsequently, these isolated fault patches were linked laterally during the late Chattian to early

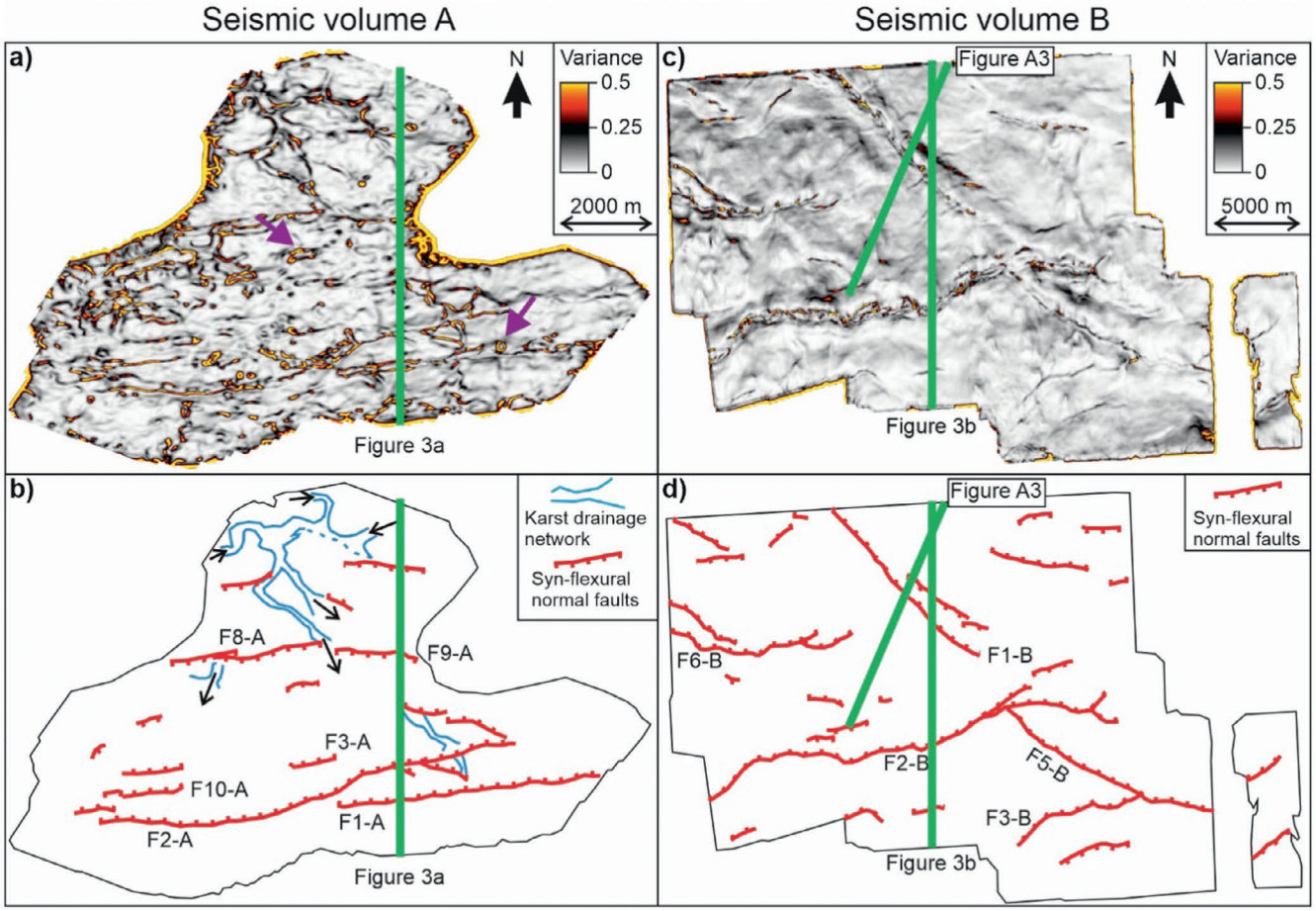

FIGURE 4 | (a) Variance attribute of the foreland unconformity reflector of seismic volume A (i.e., top of the karstified Upper Jurassic, Figure 3a). Purple arrows highlight circular variance features interpreted as sinkholes. (b) Present-day distribution of the syn-flexural fault network and the drainage network of the karstified Upper Jurassic, interpreted based on the variance attribute shown in the panel above. Black arrows indicate the assumed drainage direction of the palaeokarst network. (c) Variance attribute of the foreland unconformity reflector of seismic volume B (i.e., top of the late Cretaceous; Figure 3b). (d) Present-day distribution of the syn-flexural normal fault network in seismic volume B, interpreted from the variance attribute of the foreland unconformity shown in the panel above.

Burdigalian without further lengthening of the fault (T-x profiles in Figure 5a,b). This evidences lateral fault growth according to the isolated fault growth model (Figure A1). The throw minima and maxima along the fault do not show (major) lateral shifts (T-x profiles in Figure 5a,b), implying a dominant dip-slip component during the fault evolution. The T-z profiles along these faults are dominantly characterised by B- and D-shapes (Figure 5a,b). This suggests vertical fault growth followed the isolated or dip-linkage fault growth styles (Figure A2).

Early Chattian fault segments all record throw maxima for the foreland unconformity reflector down-dip the fault (T-z profiles 1–3, 5, 6 and 9 in Figure 5a and T-z Profiles 1, 3–7, 9 and 10 in Figure 5b). This suggests that these fault segments nucleated at the top of the Mesozoic basement at the onset of flexure. This shallow nucleation is also reflected in the EI values for the early Chattian exceeding 1 in these T-z profiles (T-z profiles 1–3, 5, 6 and 9 in Figure 5a and T-z profiles 1, 3–7, 9 and 10 in Figure 5b), which suggests that the fault was surface breaking shortly after nucleation during this time. Both the base karstified Upper Jurassic and top Baustein Beds reflectors record lower throw values compared to the foreland unconformity reflector for these T-z profiles (T-z profiles 1–3, 5, 6 and 9 in Figure 5a and T-z profiles 1, 3–7, 9 and 10 in Figure 5b). This evidences that nucleation was followed by both up- and downward propagation of the fault (Figure A2).

Fault patches that developed later due to lateral growth have T-z profiles with D-shapes, with throw maxima recorded by the top Baustein Beds or top Cyrena Beds reflectors (T-z profiles 7, 8 and 10 in Figure 5a and T-z profiles 2 and 8 in Figure 5b). Reflectors directly above and below these throw maxima record lower throw values (T-z profiles 7, 8 and 10 in Figure 5a and T-z profiles 2 and 8 in Figure 5b). This suggests that these fault segments nucleated within the basin fill during flexure, followed by up- and downward propagation (Figure A2).

Between 1700 and 2700 m along F1-A, the fault was inactive during the late Chattian to early Aquitanian (T-x profile in Figure 5a). Here, the T-z profiles have B-shapes with a second, shallow throw maximum recorded by the top Cyrena Beds reflectors (T-z profiles 5, 6 and 9 in Figure 5a). This indicates that late Chattian to early Aquitanian inactivity was followed by late Aquitanian to early Burdigalian nucleation at the top of

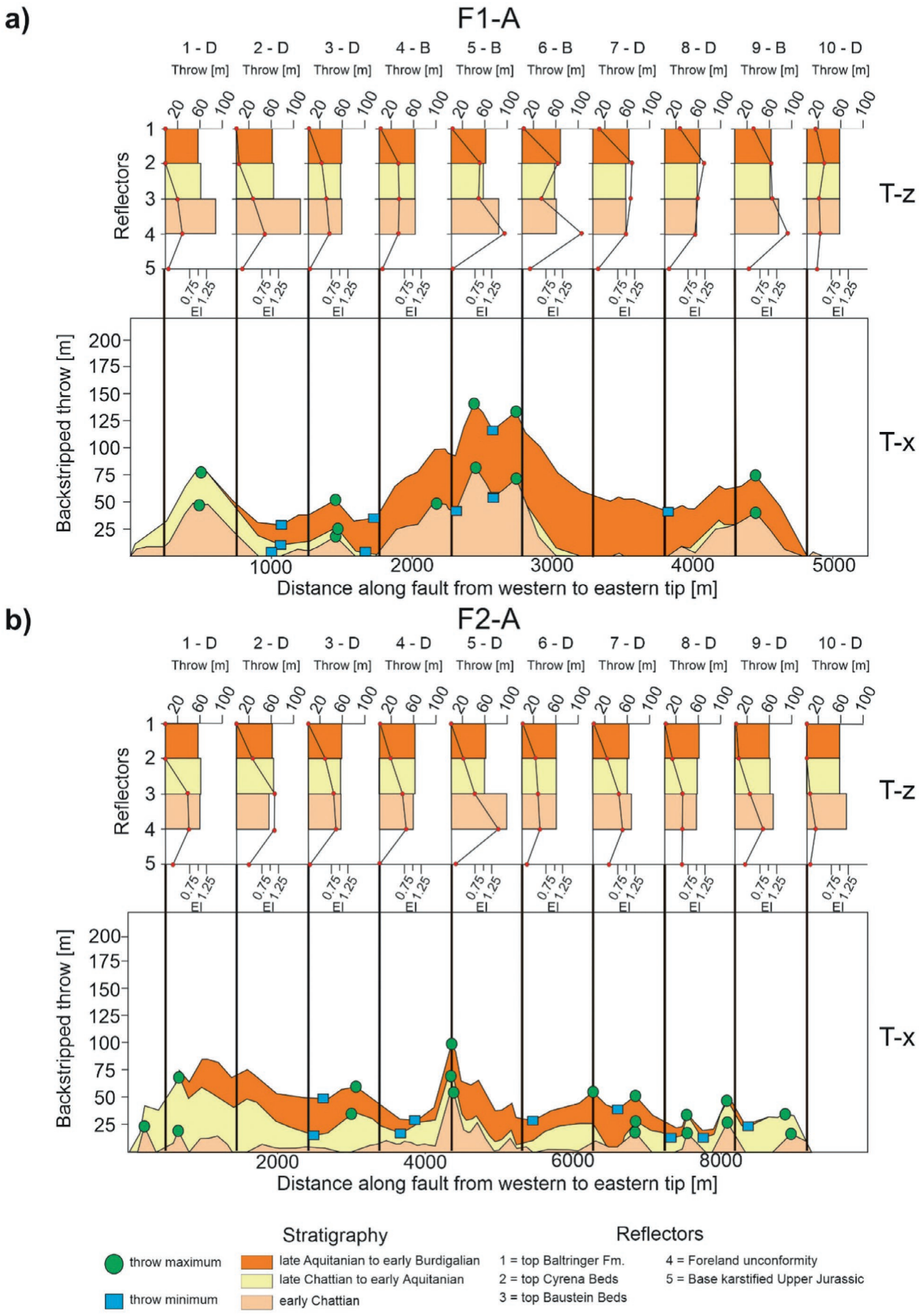

FIGURE 5 | Backstripped T-x profile with 10 T-z profiles along the length of faults (a) F1-A and (b) F2-A. EI values of the different seismic-stratigraphic units are given in coloured boxes in the T-z profiles.

the Cyrena Beds. Subsequent downward propagation led to dip-linkage with the formerly inactive lower segment (Figure A2).

4.1.2 | Syn-Flexural Normal Faults Growing According to the Constant-Length Fault Growth Model

Fault F1-B attains its final fault length during the first phase of fault growth (T-x profile in Figure 6). This indicates lateral fault growth followed the constant length model (Figure A1). Like F1-A and F2-A, throw minima and maxima along the back-stripped T-x profile do not show (major) lateral shifts (T-x profile in Figure 6). T-z profiles along the fault are dominantly characterised by either B- or D-shapes (Figure 6), which implies a mix of dip-linkage and isolated fault growth (Figure A2).

The foreland unconformity reflector records a throw maximum in all T-z profiles along the fault (Figure 6). Both the deeper top Turonian and shallower top Rupelian reflectors record lower throw values than the foreland unconformity reflector (T-z profiles in Figure 6). This implies that this fault nucleated at the top of the Mesozoic basement at the onset of flexure and subsequently propagated both up and downward (Figure A2). This corroborates with EI values higher than 1 for the late Eocene to Rupelian stratigraphy (Figure 6), implying the fault was surface breaking shortly after nucleation. This early fault growth pattern resembles that observed for F1-A and F2-A (Section 4.1.1). Furthermore, nucleation at the top of the Mesozoic basement implies that the lower segment that bounded the Palaeozoic to Triassic Giftthal Through (Figure 3b; Bachmann and Müller 1991; Eskens et al. 2024), located at 480 m depth at the onset of flexure (Figure A3), was not reactivated during flexure.

F1-B is characterised by a phase of inactivity during the early to middle Chattian along its western half (Figure 6, from 500 to 5500 m along the backstripped T-x profile). This is reflected in the T-z profiles having B-shapes with a second shallow throw maximum recorded by the top Chattian Sands reflector (T-z

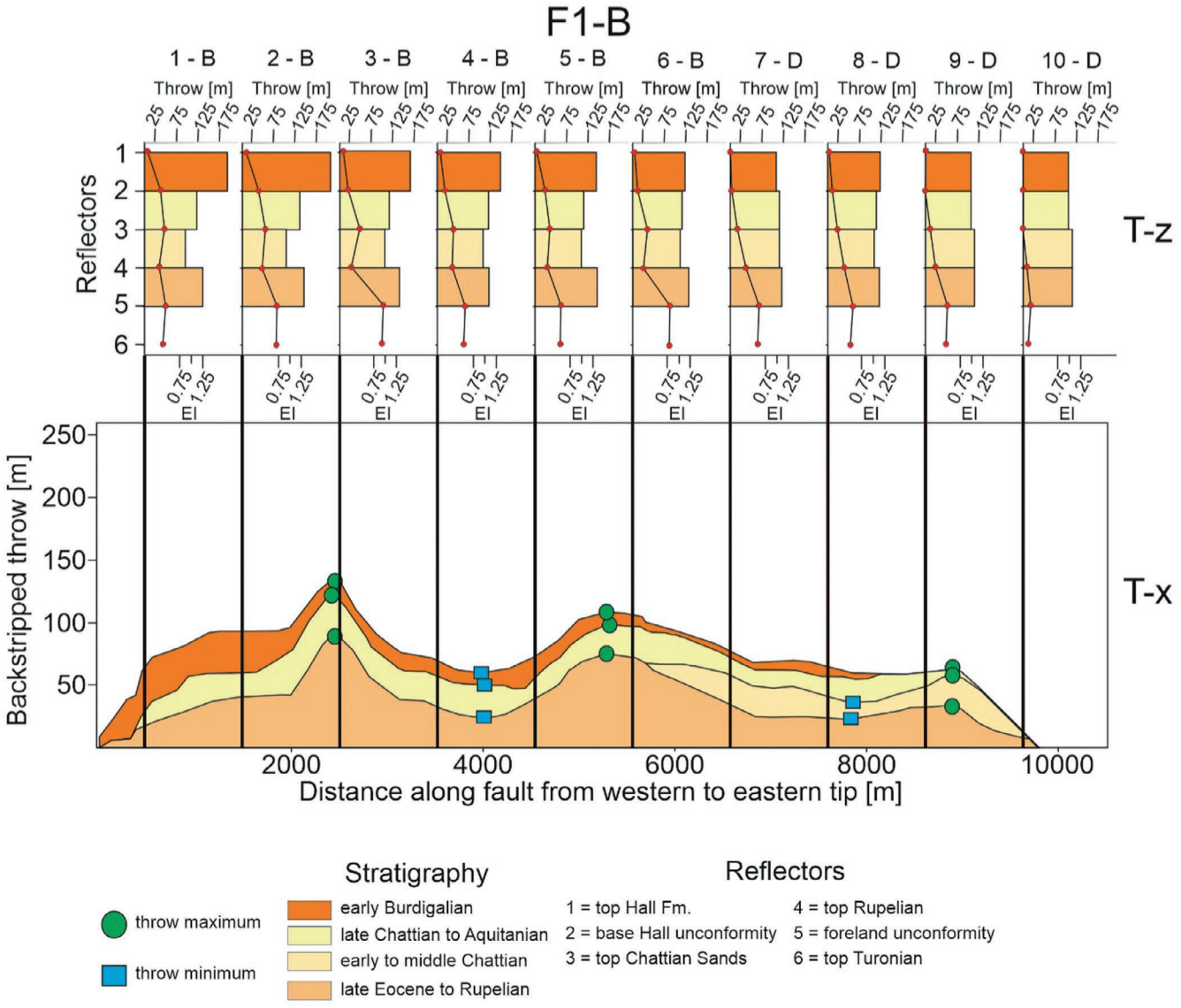

FIGURE 6 | Backstripped T-x profile with 10 T-z profiles along the length of fault F1-B. EI values of the different seismic-stratigraphic units are given in coloured boxes in the T-z profiles.

Profiles 1–6 in Figure 6). This implies that the early to middle Chattian phase of inactivity was followed by nucleation of an upper segment at the top of the Chattian Sands during the late Chattian (Figure A2). Subsequently, this upper segment dip-linked with the lower, formerly inactive segment. This reflects fault growth styles observed for F1-A and F2-A (Section 4.1.1).

Along the eastern end of the fault, the T-z profiles have D-shapes for which lower throw values are recorded for successively younger syn-flexural reflectors (Figure 6, from 5500 to 9500 m along backstripped T-x profile). This evidences that the eastern end of this fault was characterised by growth faulting (Figure A2) following the late Eocene to Rupelian nucleation at the top of the Mesozoic basement.

4.1.3 | Syn-Flexural Normal Faults Growing According to the Hybrid Fault Growth Model

Late Eocene and Rupelian fault growth was characterised by the development of laterally isolated fault patches along fault F2-B (T-x profile in Figure 7). This was followed by early to middle Chattian inactivity along most of the fault (T-x profile in Figure 7). Subsequent reactivation during the late Chattian to Aquitanian led to lateral linkage along the eastern fault segment, throw accumulation and 1.5 km westward tip propagation along the western segment (T-x profile in Figure 7). This evidences that this fault grew laterally following the hybrid growth model (Figure A1).

T-z profiles are dominated by B- and D-shapes (Figure 7). This evidences that vertical growth of F2-B was dominantly characterised by isolated growth or dip-linkage of a lower- and upper-fault segment (Figure A2). Patches where fault growth initiated during the late Eocene to Rupelian record throw maxima for the foreland unconformity and top Turonian reflectors (T-z profiles 2–7, 9 and 10 in Figure 7). In the case of the foreland unconformity recording a throw maximum, the deeper top Turonian and shallower top Rupelian reflectors record lower throw values (T-z Profiles 2–7 in Figure 7). This means that initial fault nucleation of these patches occurred at the top of the Mesozoic basement, followed by up- and downward propagation (Figure A2). This corresponds with EI >1 for the late Eocene to Rupelian stratigraphy (Figure 7), indicating these segments were surface-breaking shortly after nucleation during this time. Conversely, the upward throw decrease from the top Turonian reflectors towards the foreland unconformity and top Rupelian reflectors along the eastern segment (T-z Profiles 9 and 10 in Figure 7) suggests a Mesozoic fault was reactivated. However, EI >1 for late Eocene to Rupelian stratigraphy along this segment indicates that this part of the fault also reached the surface shortly after reactivation.

Fault patches that developed later due to lateral growth have T-z profiles with B- and D-shapes for which the top Chattian Sands and top Rupelian reflectors record throw maxima (T-z Profiles 1 and 8 in Figure 7). This suggests that these segments started developing after the initial onset of flexure and nucleated within the basin fill (Figure A2). Furthermore, along segments where the fault was inactive during the early to middle Chattian, the T-z profiles are characterised by B- and Z-shapes (T-z Profiles 2–7 and 9 in Figure 7). The Z-shaped T-z profiles indicate that reactivation occurred through upward propagation of the segment sealed during inactivity (Figure A2). Alternatively, the B-shaped T-z profiles indicate an upper segment nucleated within the basin fill that subsequently dip-linked with the lower segment that was previously sealed (Figure A2).

5 | Discussion

Our data reveal growth styles, kinematics, and the distribution of the offsets of late Eocene to early Miocene syn-flexural normal faults in the German Molasse Basin. First, we discuss the implications of our quantitative analysis in terms of 4D syn-flexural normal fault growth in the German Molasse (Section 5.1). Subsequently, we identify agreements and discrepancies of syn-flexural fault growth in the entire Molasse Basin and discuss the implications thereof (Section 5.2). Lastly, we discuss the spatio-temporal variations in syn-flexural normal fault growth styles in the Molasse Basin in terms of mechanism(s) that controlled the flexure of the European plate during the Alpine orogeny (Section 5.3).

5.1 | The Nucleation and Growth Styles of Seismic-Scale Normal Faults in the German Molasse Basin

In our data volumes, the syn-flexural normal faults have an E-W/SW-NE strike (sub)parallel to the orogenic front (Figure 4), in agreement with previous studies in the German Molasse (e.g., von Hartmann, Tanner, and Schumacher 2016; Budach et al. 2018; Mraz et al. 2018; Shipilin et al. 2020). This reaffirms that these faults grew in response to flexure-related extensional stresses around the forebulge migrating in front of the orogen. Additionally, it reflects the results from analogue (Supak, Bohnenstiehl, and Buck 2006) and numerical (von Hartmann, Tanner, and Schumacher 2016) experiments. Faults in our data volumes that deviate from the general trend are NW-SE oriented and represent either relay faults connecting fault segments (e.g., F5-B; Figure 4c,d) or are related to pre-existing faults (F1-B; Figure 4c,d; Bachmann and Müller 1991; Eskens et al. 2024). The lack of a correlation between karst features and normal fault locations (Figure 4b) implies that karst, in this case, did not act as a pre-existing weakness localising deformation. Furthermore, the throw minima and maxima barely shifting laterally along the fault planes (T-x profiles in Figures 5–7) suggest little to no oblique-slip on the faults. F1-B, presently striking oblique to the Alpine thrust front, may currently experience oblique slip. However, our data show no evidence for this. Instead, our results represent the minimum throw values along these faults. Furthermore, in our study area, Riedel shears, which would be associated with oblique slip along the faults, are not observed in the variance slices of the foreland unconformity (Figure 4), as seen in other basins where faults are affected by oblique slip (e.g., Balázs et al. 2018, their figure 12c). The onset of flexural subsidence (late Eocene to Rupelian and early Chattian for volumes A and B, respectively) led to the nucleation of new fault patches at the top of the pre-flexural basement (Figures 5–7).

This suggests that the highest strain related to the extensional stress resulting from bending around the forebulge was localised

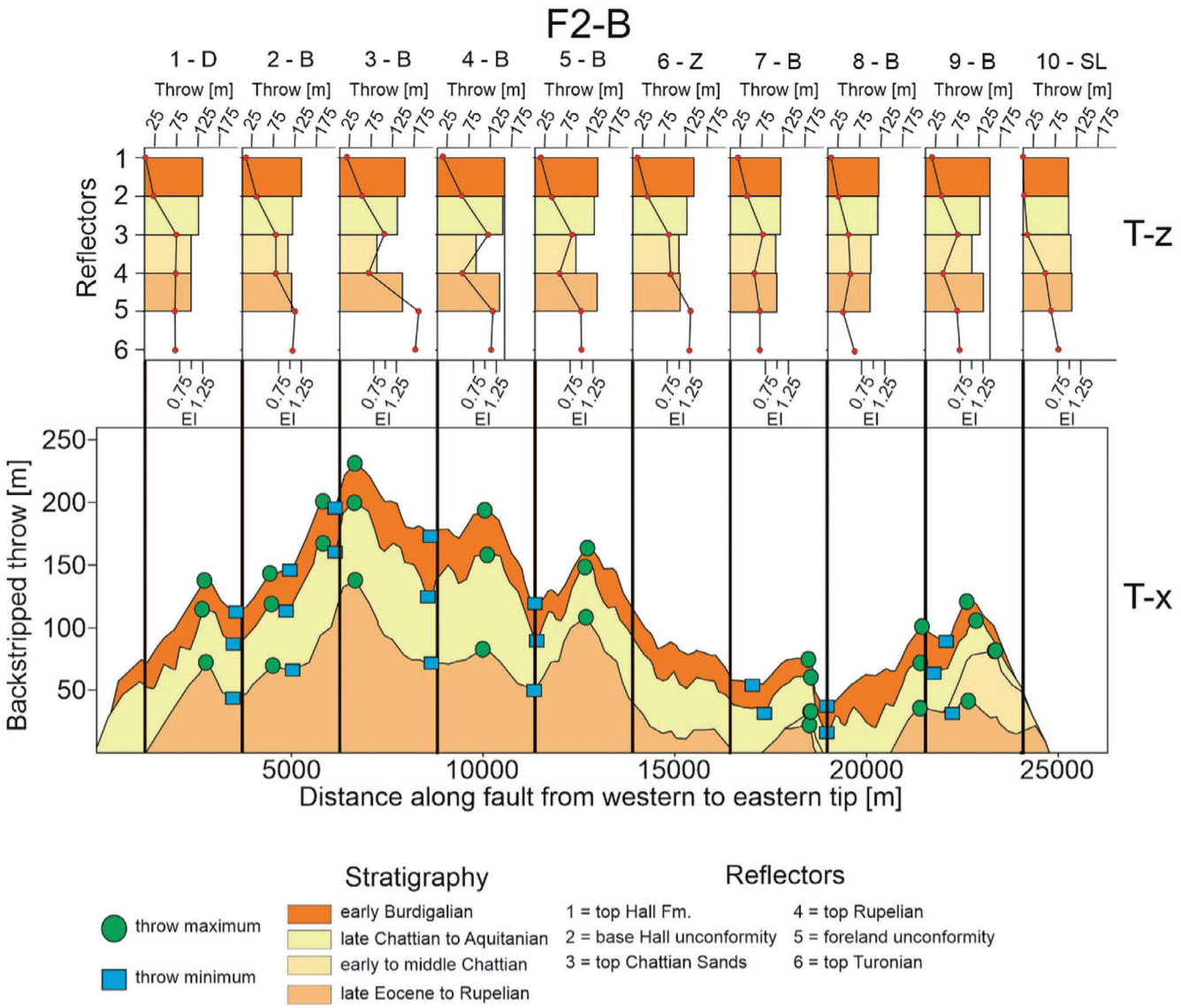

FIGURE 7 | Backstripped T-x profile with 10 T-z profiles along the length of fault F2-B. EI values of the different seismic-stratigraphic units are given in coloured boxes in the T-z profiles.

close to or at the surface of the European plate, as observed in other convergence systems and modelling studies (Supak, Bohnenstiehl, and Buck 2006; Langhi, Ciftci, and Borel 2011). However, higher throw values for Mesozoic basement reflectors compared to the foreland unconformity or basin-fill reflectors for some faults (T-z Profiles 8–10 in Figure 7, T-z Profiles 1–6 in Figure A4b and T-z Profiles 2–10 in Figure A5b) imply reactivation of Mesozoic pre-flexural faults. Therefore, flexure was associated with both the reactivation of pre-existing faults and the nucleation of a new fault network. This agrees with previous studies in the German Molasse (von Hartmann, Tanner, and Schumacher 2016; Budach et al. 2018; Mraz et al. 2018; Shipilin et al. 2020).

Whereas reactivated faults grew laterally following the constant length model (T-x profiles of F9-A and F5-B; Figures A4b and A5b), newly nucleated faults follow the isolated or hybrid fault growth models (T-x profiles in Figures 5 and 7). This implies that reactivation promoted rapid lengthening, a process that is also observed in rift basins (Walsh, Nicol, and Childs 2002; Giba, Walsh, and Nicol 2012; Whipp et al. 2014; Rotevatn et al. 2018). Furthermore, linkage segments are characterised by nucleation within the syn-flexural basin fill (e.g., T-z Profiles 7 and 8 in Figure 5a and T-z Profiles 2 and 8 in Figure 5b). This implies that the fault tip migrated stratigraphically upward during the lateral growth of newly nucleated faults (Figure 8). Fault segments characterised by inactivity and subsequent reactivation during flexure were observed to correspond with T-z profiles with either B- or Z-shapes (e.g., T-z Profiles 5 and 6 in Figure 5a, T-z Profiles 1–6 in Figure 6 and T-z Profiles 2 to 7 and 9 in Figure 7). The first suggests that new segments could nucleate within the basin fill during ongoing flexure and subsequently dip-link with the sealed lower segments (Figure 9). This was also observed by previous authors (von Hartmann, Tanner, and Schumacher 2016; Shipilin et al. 2020). The latter implies that, alternatively, the buried segments were reactivated and propagated upward.

Interestingly, F1-B grew laterally following the constant-length model even though it nucleated newly at the top of the Mesozoic basement at the onset of flexure. This indicates that even though

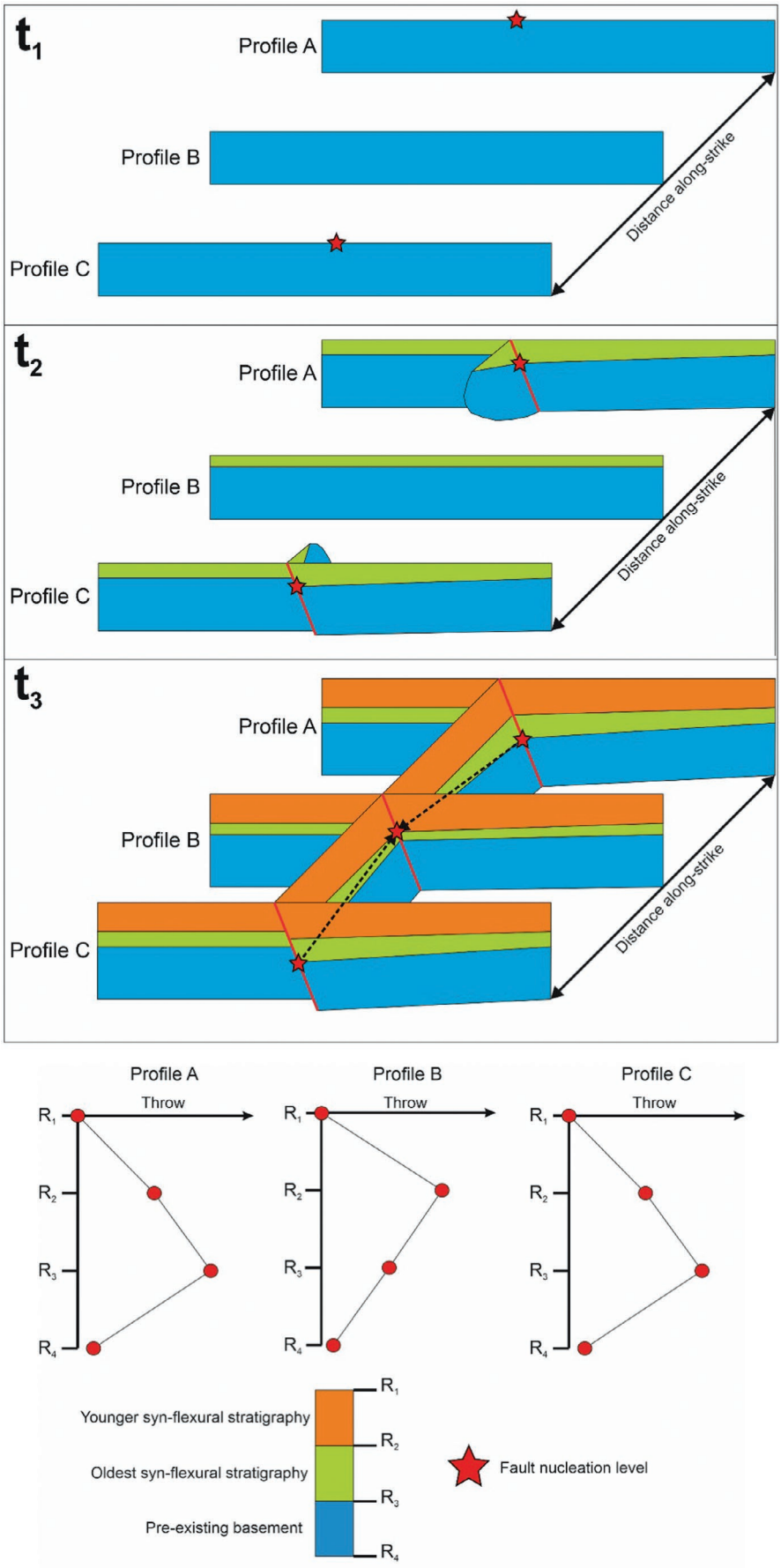

FIGURE 8 | Legend on next page.

FIGURE 8 | Schematic illustration of nucleation and subsequent isolated lateral growth of syn-flexural normal faults as observed in the German Molasse basin, where R_1–R_4 indicate the seismic-stratigraphic reflectors. $\mathbf{t_1}$, The normal fault nucleates along profiles A and C, whereas initiation of fault growth along profile B is delayed. At this time, syn-flexural sediment thickness is negligible. $\mathbf{t_2}$, Sedimentation contemporaneous with fault activity along profiles A and C results in syn-kinematic thickening. However, the fault has not laterally propagated to the position of profile B, so the coevally deposited sediments in profile B are thinner and do not record fault-related thickening. $\mathbf{t_3}$, Continued upward propagation of the fault in profiles A and C results in thickening the youngest syn-flexural stratigraphy. Furthermore, due to lateral fault growth, the sediments deposited along profile B will also record fault-related thickening. This indicates that the fault tip migrated laterally and stratigraphically upward (indicated by the black dashed line). In T-z profiles along the fault, the throw maximum is therefore observed to be recorded at different stratigraphic levels.

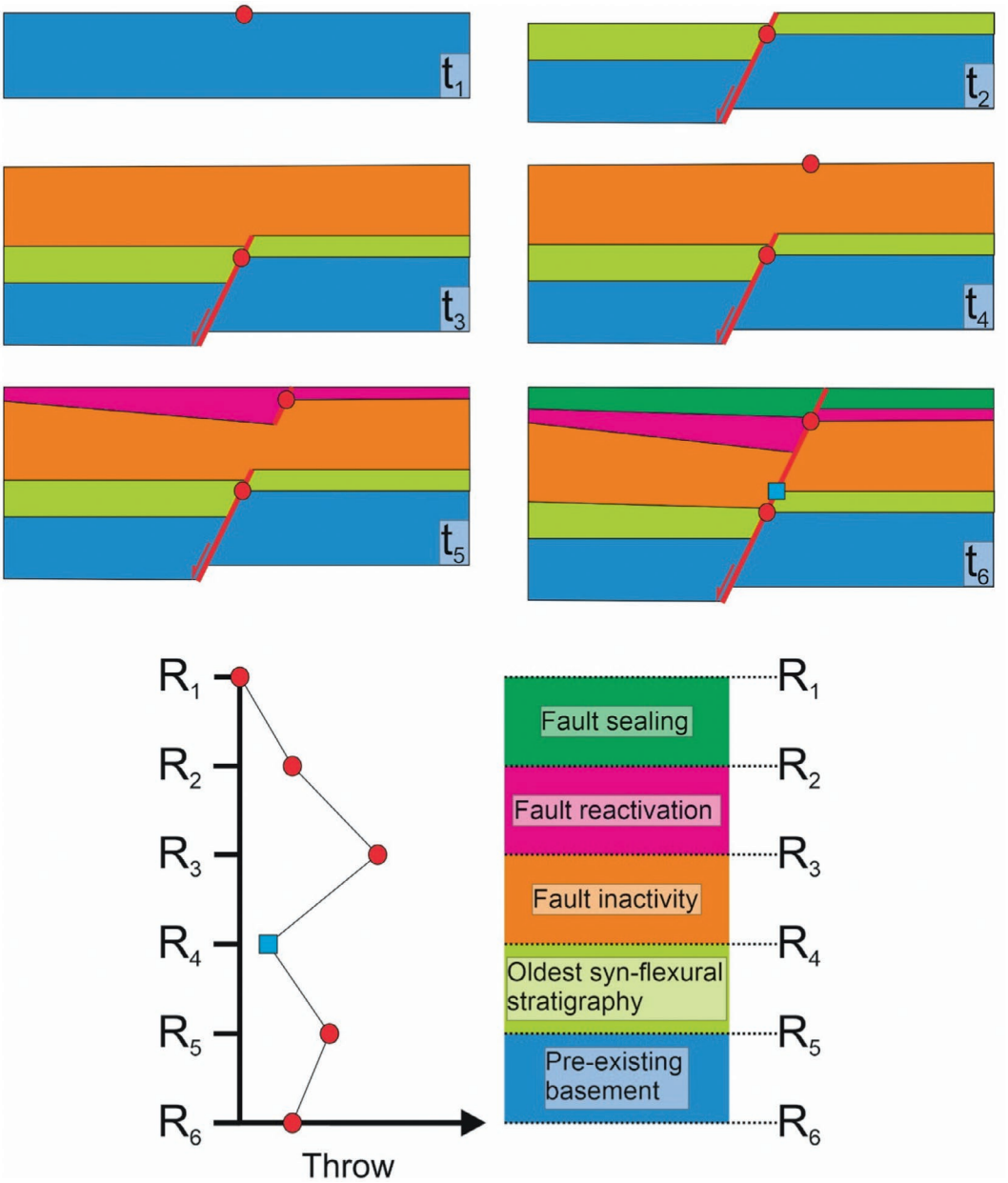

FIGURE 9 | Schematic representation of the development of vertically linked faults in the German Molasse and their resultant T-z profile along a vertically linked segment. $\mathbf{t_1}$, Fault growth nucleates at the top of the pre-existing basement at the onset of flexural subsidence, when no syn-flexural sediments have been deposited. $\mathbf{t_2}$, Ongoing flexural subsidence leads to the development of a normal fault that grows both downward into the pre-existing basement and upward in the syn-flexural basin fill, recorded as syn-kinematic thickening. $\mathbf{t_3}$, Fault growth ceases, with the remnant topography being filled by sediments. $\mathbf{t_4}$, Renewed tectonic activity leads to the nucleation of an upper segment at the top of the syn-flexural basin fill instead of the deeper segment being reactivated. $\mathbf{t_5}$, The new fault grows downward into the syn-flexural fill that was initially unaffected by faulting, and upward into the newly deposited sediments. $\mathbf{t_6}$, Downward propagation of the fault leads to vertical linkage at the upper tip of the lower fault segment, while upward growth leads to syn-kinematic thickening of newly deposited sediments. Finally, the fault is sealed.

the Palaeozoic segment was not reactivated, it may have localised deformation in its cover. As a result, this forced the deviating NW-SE strike and rapid lengthening of F1-B. Nucleation of new faults above pre-existing basement faults rapidly attaining their final length was also found by previous authors in the German Molasse (Faults GartenbergS and Gelting N; Shipilin et al. 2020), as well as in the Timor Through subduction trench (Langhi, Ciftci, and Borel 2011). This suggests that pre-flexural faults buried at greater depth at the onset of flexure were not reactivated during flexure. Instead, basement faults may have lowered the required strain to nucleate a syn-flexural fault in its cover.

5.2 | Syn-Flexural Normal Faults in the Molasse Basin

Previous authors identified syn-flexural normal faults in the Swiss Molasse that nucleated close to the top of the pre-existing basement during flexure, subsequently linking at depth with pre-flexural Mesozoic faults (Roche et al. 2020, their figures 10 and 11). Similarly, T-z profiles of faults interpreted by previous authors in the Austrian Molasse (Gross et al. 2015; Masalimova et al. 2015) also indicate nucleation at the top of the Mesozoic basement, within the syn-flexural basin fill, and reactivation of Mesozoic basement faults (Figure A6). Therefore, the nucleation and growth patterns in the Swiss- and Austrian Molasse reflect the findings of this and previous studies in the German Molasse (Section 5.1). This suggests that the growth styles of the syn-flexural faults were homogeneous in the entire Molasse Basin. Furthermore, our data from the German Molasse show that the strike of syn-flexural normal faults may deviate from the general E-W trend, that is, parallel to the orogenic front, in cases where they are related to pre-existing structures (e.g., F1-B; Figure 4c,d). Moreover, syn-flexural faults that developed close to either pre-existing highs (Landshut-Neuötting High and Bohemian Massif; Figure 1) or basins (F1-B of the Giftthal Trough, this study; Unterlören Graben, Heuberger et al. 2016) do not necessarily strike (sub)parallel to the orogenic front. This suggests that pre-flexural structures incorporated in the autochthonous foreland basin, or located at its margin, exert an important local control on the local strain partitioning, thereby governing the strike of syn-flexural normal faults.

Combining our data with that of previous authors shows that the cumulative syn-flexural offsets increase from north to south (Figure 10a). This implies the magnitude of flexure increased towards the south, which corroborates the southward deepening of the basin during ongoing flexure (e.g., Lemcke 1988; Bachmann and Müller 1991). More striking, however, is that the cumulative syn-flexural offsets increase from the Western to the Eastern German Molasse on both the distal margin and the axial part of the basin (Figure 10a). This suggests an increase in the magnitude of strain accommodated by syn-flexural faults in the Eastern German Molasse compared to the Western German Molasse. Zhang et al. (2023) showed, using a 3D flexural model, that a lateral increase in the deflection of a subducting oceanic plate leads to an increase in the magnitude of extensional stresses in the same direction as the increasing flexure. Taking this as an analogue, the increase in the extensional strain accommodated in the Eastern German Molasse was likely facilitated by an increase in the deflection of the European plate towards the east. This interpretation corroborates the late Oligocene to early Miocene along-strike deepening of the depositional environments from the Western German to the Eastern German Molasse Miocene (e.g., Lemcke 1988; Sissingh 1997; Kuhlemann and Kempf 2002). Furthermore, syn-flexural normal faults further north of the orogenic front are sealed by progressively younger stratigraphy (Eskens et al. 2024). We interpret this migration to have resulted from the northward advance of the forebulge and the associated extensional stress and strain field as the Alps continued encroaching the European margin.

The growth of syn-flexural normal faults in the vicinity of the Alpine front in the Western German Molasse began during the early Rupelian (Figure 1, Mraz et al. 2018). Their counterparts 35 km to the north started developing later, during the early Chattian (ca. 27.5 Ma, seismic volume A; Figures 1 and 5). This gives us an average northward migration rate of 7.8 mm/year for the flexural forebulge during the early Oligocene. This is comparable to the northward propagation rates of the Alpine wedge based on (1) the onlap patterns of the basal limestones (8.5–12.9 mm/year; Sinclair 1997b), (2) restoration of geological cross-sections (at least 5.5–4.5 mm/year; Schmid et al. 1996) and (3) plate tectonic reconstructions (6–8.9 mm/year; Handy, Ustaszewski, and Kissling 2015; Van Hinsbergen et al. 2020; Le Breton et al. 2021). This suggests that, similar to how normal faults are used for tracing the migration of the extensional stress field due to slab rollback in a back-arc basin (Giba, Nicol, and Walsh 2010), syn-flexural normal faults in a foreland basin can be used to reconstruct the spatiotemporal location of the forebulge.

5.3 | Syn-Flexural Normal Faults as Fingerprints of the Geodynamic Evolution of the Alpine Orogeny

Our new data, combined with previous work, identifies an eastward increase in the European plate flexure and, thereby, basin subsidence during the Oligocene-Early Miocene evolution of the Molasse Basin (Jin et al. 1995; Zweigel, Aigner, and Luterbacher 1998; Kuhlemann and Kempf 2002). Such along-strike variations in foreland plate flexure are often interpreted to be induced by lateral variations in the strength of the downgoing plate (Beaumont 1981; Waschbusch and Royden 1992; Burov 2010), plate coupling (Ziegler, Bertotti, and Cloetingh 2002; Willingshofer and Sokoutis 2009) and loading from slabs, thrusts and sediments (Flemings and Jordan 1990; DeCelles and Giles 1996; Sinclair 1997a; DeCelles 2012; Fosdick, Graham, and Hilley 2014).

Using thermomechanical and elastic modelling, previous studies showed that the thickness of the lithospheric mantle, which contributes 70% to the integrated lithospheric strength, decreases from the Western to the Eastern German Molasse (Spooner et al. 2022). This is translated into a present-day reduction in the strength of the European lithosphere in the same direction (Figure 11a; Andeweg and Cloetingh 1998; Spooner et al. 2022). As lithospheric strength 'is frozen in' (Watts and Burov 2003), we can assume that the present-day strength of the European lithosphere is representative of the conditions during the Oligocene to early Miocene. This assumption is supported by the

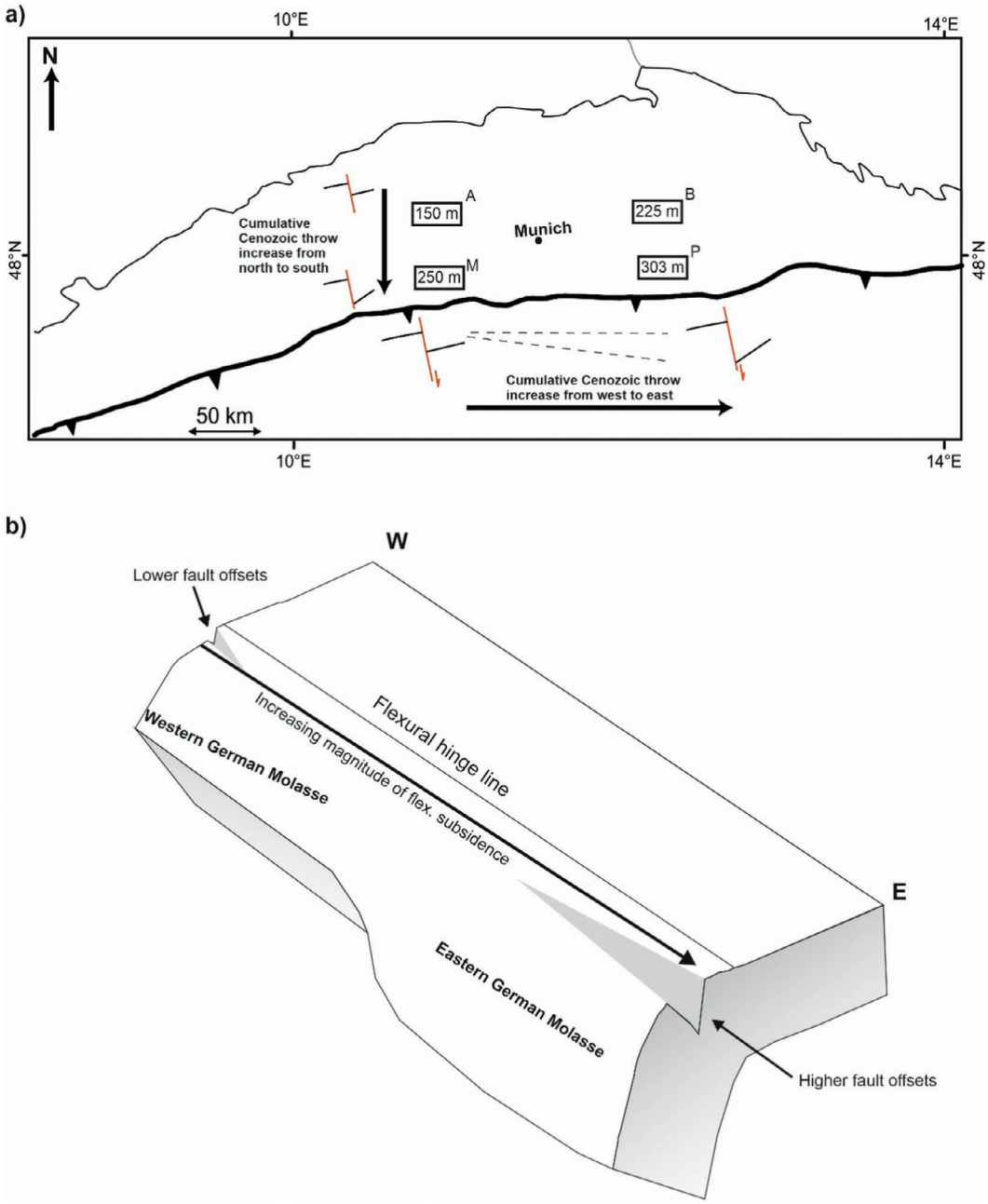

FIGURE 10 | (a) Magnitude of maximum cumulative syn-flexural offsets down-dip of the normal faults in the German Molasse Basin, based on data presented in this work and from previous studies (Cordero Peña 2007; Mraz et al. 2018, denoted as **P** and **M**, respectively). **A** = seismic volume A presented in this study, **B** = seismic volume B presented in this study. For deriving the syn-flexural throw values from the time to the depth from time-domain data from Cordero Peña (2007), see Section A.1. (b) Because of an eastward increase in the magnitude of flexural subsidence of the European lithosphere during the Alpine orogeny, the cumulative offsets down-dip of the syn-flexural normal faults are higher in the Eastern German Molasse compared to the Western German Molasse. The normal fault offsets are not shown to scale relative to the foreland plate. Inspired by Zhang et al. (2023).

similarity in estimates of the European lithospheric strength beneath the Alpine wedge for both the present-day (Willingshofer and Cloetingh 2003) and the Oligocene (Pfiffner, Schlunegger, and Buiter 2002). Lithospheric strength is one of the factors dictating the magnitude and wavelength of the flexural profile of a foreland basin (Flemings and Jordan 1989; Waschbusch and Royden 1992). Therefore, we interpret the observed eastward increase in deflection of the European plate and related eastward increase in cumulative syn-flexural normal fault offsets (Section 5.2) as a fingerprint of this lateral strength variation of the European lithosphere. This suggests that the magnitude of foreland basin deflection was higher where the foreland lithosphere was weaker. A similar cause-and-effect relationship is also observed in the Polish Carpathian foreland basin, where syn-flexural fault offsets are higher in the eastern foreland basin, which developed above the Tornquist-Teisseyre Zone (Palaeozoic suture, i.e., a lithospheric weak zone; Narkiewicz et al. 2015; Smit, Wees, and Cloetingh 2016), compared to the

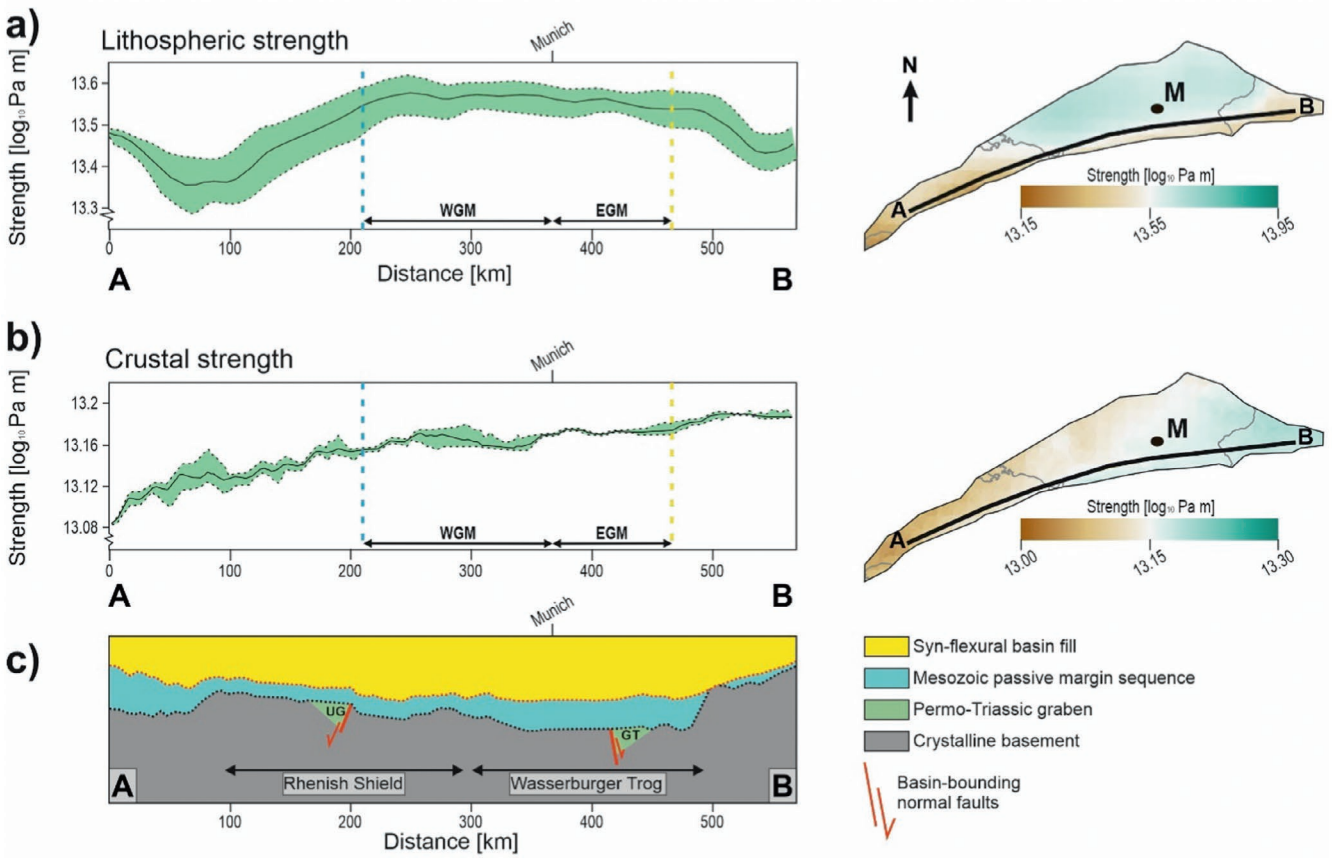

FIGURE 11 | A 20-km-wide swath profile of the present-day showing: (a) integrated lithospheric strength (crust and lithospheric mantle) and (b) crustal strength in the Molasse Basin along profile AB (Spooner et al. 2022). The vertical blue dashed line indicates the border between the Swiss and German Molasse, whereas the yellow vertical dashed line is the border between the German and Austrian Molasse. EGM, Eastern German Molasse; WGM, Western German Molasse; M, Munich. (c) Crustal section along profile AB, indicating the location of the pre-flexural Rhenish Shield and Wasserburger Trog. Adapted from Eskens et al. (2024). GT, Giftthal Through; UG, Unterlören Graben.

western foreland basin that developed on the Western European Platform (Krzywiec 2001).

In contrast to the lithospheric strength, crustal strength increases from the Western to the Eastern German Molasse Basin (Figure 11b; Spooner et al. 2022). Spooner et al. (2022) interpret this to be the result of a cooler crustal geotherm in the Eastern German Molasse. Furthermore, the local variations in the crustal strength correspond to the variations in the European passive margin architecture, that is, lower strength is estimated for the area of the Rhenish Massif, whereas higher strength is calculated for the Wasserburger Trog (Figures 11b and 11c). The paradox of an eastward increase in crustal strength parallel with an increase in the magnitude of flexure (Subsection 5.2) suggests that the distribution of crustal strength was not a primary factor controlling the magnitude of foreland plate flexure. Instead, the effect of the lithospheric strength prevails. However, it is noteworthy that the magnitude of flexure increases south of the Bohemian Massif, which delimits the Eastern Molasse to the north. As Andeweg and Cloetingh (1998) suggested, this may have resulted from the downward squeezing of the European plate between the approaching Eastern Alpine wedge and the Bohemian Massif acting as a buttress. Consequently, subsidence had to be accommodated over a smaller area, which may have contributed to the higher magnitude of flexure of the European plate towards the east (Section 5.2). Inherently, the eastward increase in deflection of the European plate likely led to a shortening of the wavelength and an increase in the amplitude of the flexural profile in the Eastern German Molasse, consistent with the weaker foreland lithosphere (Figures 11a and 12a). Consequently, this would lead to an eastward narrowing of the zone experiencing extensional strain (Figure 12b), which should be expressed in the spatiotemporal pattern of syn-flexural fault activity. During the early Chattian to early Burdigalian, fault activity is recorded in both the basin axis (Mraz et al. 2018) and the distal margin (Eskens et al. 2024) of the Western German Molasse. In contrast, coeval activity in the Eastern German Molasse was restricted to the distal margin (Eskens et al. 2024). This suggests an eastward decrease in the width of the zone accommodating extensional deformation, following the eastward plate weakening, consistent with our model (Figure 12).

It is noteworthy that lateral variations in the lithospheric and/or crustal strength, which induce along-strike variable amounts of the foreland plate flexure, may arise from several factors, such as: (1) pre-existing weaknesses (e.g., Willingshofer, Sokoutis, and Burg 2005; Roure 2008; Calignano et al. 2015), (2) passive margin irregularity (i.e., promontories and embayments; Lash 1988; Maiti et al. 2024) and/or (3) margin obliquity (Maiti et al. 2024).

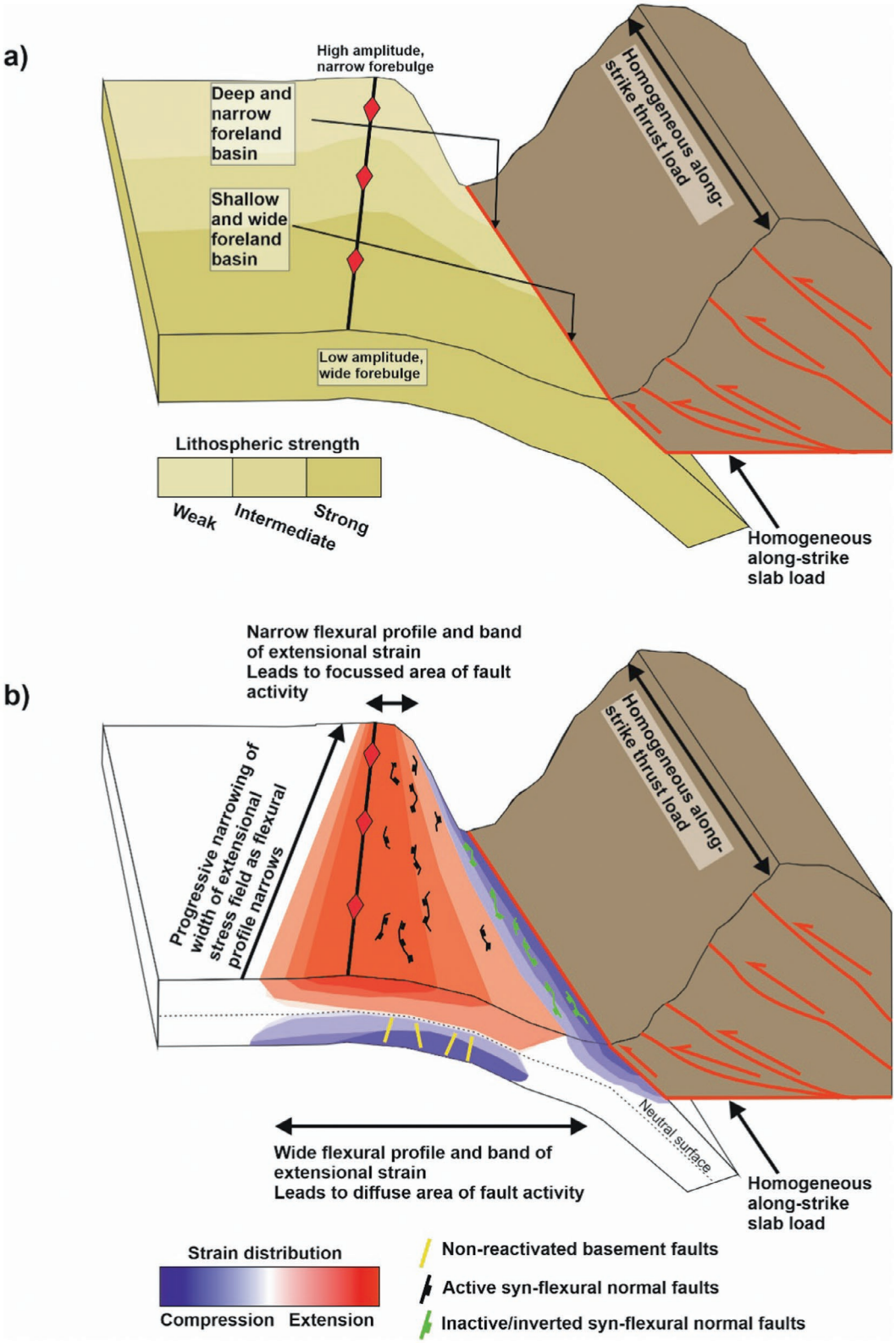

FIGURE 12 | (a) Schematic model of the flexure of a foreland plate with along-strike variable lithospheric strength. Note that orogen-parallel variations in (sub)surface loads, plate coupling or the presence of pre-flexural structures in the foreland are not accounted for in this model. (b) Where the flexural wavelength is narrow, the zone of extensional stresses around the forebulge is more focused. On the contrary, where the flexural profile is wide, the zone of extensional stresses is more diffuse. Close to the orogenic front, compressive stresses are dominant.

In all these cases, the continental lithosphere of laterally variable strength would be involved in the collision, leading to along-strike variations in the foreland plate flexure (assuming laterally constant loads). Therefore, it is likely that the along-strike heterogeneity in the architecture of the European lithosphere, represented by the continental Briançonnais terrane

(in front of the Western and Central Alps), which laterally transitioned into the oceanic Penninic domain (in front of the Eastern Alps, e.g., Faupl and Wagreich 2000; Mohn et al. 2014; Rosenberg et al. 2021), induced lateral strength variations in the European plate. As such, the inherited Mesozoic architecture of the European plate may have been expressed in lateral variations in foreland flexure and, thereby, syn-flexural normal fault growth in the Molasse Basin. This emphasises the importance of lithospheric memory in the development of foreland basins.

During the Oligocene to early Miocene, the proximal foreland deposits were accreted to the base of the Alpine wedge to form the German Subalpine Molasse (Hinsch 2013; Ortner et al. 2015, 2023). Further north of the present-day thrust front, Oligocene to early Miocene compressional structures are not observed. This implies that the transmission of compressive stresses was minimal, implying a decoupling between the Alpine wedge and the European foreland along the German Molasse. However, despite flexurally subsiding throughout the Miocene (Ortner et al. 2015), normal faults close to the thrust front south of Munich were inverted during the middle Miocene (Shipilin et al. 2020), and syn-flexural normal faults on the distal margin along the entire German Molasse were sealed (Figures 5–7; von Hartmann, Tanner, and Schumacher 2016; Mraz et al. 2018). This suggests enhanced effectiveness in transmitting compressional stresses from the Alpine wedge into the German Molasse Basin, which prevented continued extensional normal faulting around the forebulge from the middle Miocene onward. As Willingshofer and Sokoutis (2009) suggested, this may have resulted from a temporal change from decoupling to coupling between the orogenic wedge (Central and Eastern Alps) and the European foreland.

The present-day thickness of Molasse Basin sediments shows relative thickening from the autochthonous Western German Molasse to the autochthonous Eastern German Molasse (Ortner et al. 2023; Eskens et al. 2024). However, isopach maps from Kuhlemann and Kempf (2002) (their figure 6) suggest a higher sediment thickness in the Western Molasse during the Chattian and Aquitanian compared to the Eastern Molasse. As such, sedimentary loading was likely higher in the Western Molasse than in the Eastern Molasse at this time. This contradicts with the eastward increase in flexure, as recorded by the syn-flexural normal fault offsets (Section 5.2) and the stratigraphic architecture of the Molasse Basin (Lemcke 1988; Sissingh 1997; Kuhlemann and Kempf 2002; Schlunegger and Kissling 2022; Eskens et al. 2024). This implies that sediment loading was not the dominant force driving the foreland plate deflection.

By the Oligocene to early Miocene, the Central Alps had attained 2–4 km of topography (Frisch et al. 2001; Kuhlemann 2007; Krsnik et al. 2021). In contrast, topography in the Eastern Alps remained low until the early Miocene folding due to Adriatic indentation (Tauern Window exhumation; Kuhlemann 2007; Scharf et al. 2013; Schmid et al. 2013; Favaro et al. 2015). As a result, the Oligocene to early Miocene Central Alpine wedge was likely thicker and, therefore, heavier compared to the Eastern Alps. Consequently, the topographic load exerted by the Central Alps was likely higher than that of the Eastern Alps. Therefore, if the topographic loads were the primary control on the deflection of the European plate, the magnitude of the European plate deflection during the Oligocene to early Miocene of the Western German Molasse should have been higher compared to that beneath the Eastern German Molasse. Following the same reasoning as for the sedimentary loading above (the contradiction with the eastward increase in magnitude of flexure of the European lithosphere), this suggests that topographic loading was not the primary mechanism controlling flexure either. This decoupling between topographic loads and foreland flexure has been observed by previous authors (Schlunegger and Kissling 2015), as well as in other foreland basins, such as the Maturin Basin–Serrania thrust wedge (Jácome et al. 2003) and Carpathian (Maţenco et al. 1997) orogen-foreland systems.

Estimating the potential role of slab loading on the variations in flexure along the Molasse Basin during the Oligocene to early Miocene times is challenging. Current thermochronological, sedimentological and geological datasets have been used to suggest multiple hypotheses regarding the Alpine slab dynamics, including (multiple) slab break-offs at 35, 20 and 2 Ma (Schmid et al. 1996, 2004; Handy et al. 2010; Handy, Ustaszewski, and Kissling 2015; Fox et al. 2016), lateral slab tearing (Meulenkamp, Kováč, and Cicha 1996; Schlunegger and Kissling 2022) and a subduction polarity reversal during the early Miocene (Handy, Ustaszewski, and Kissling 2015; Eizenhöfer et al. 2023). Recent numerical modelling studies show that processes leading to lateral variations in slab pull (such as episodic slab break-off events and/or slab tearing) subsequently lead to orogen-parallel variations in loading and, thereby, along-strike variations in foreland basin subsidence (Andrić-Tomašević et al. 2023; Maiti et al. 2024). In this scenario, the still-attached part of the slab may provide a substantial load and, thereby, induce higher plate flexure than the part of the foreland basin beneath which the slab has been detached. However, evaluating the contribution of these mechanisms on the European plate deflection and subsequent syn-flexural normal fault evolution in the Molasse Basin requires further investigation.

6 | Conclusions

Here, we analysed the spatiotemporal growth of seismic-scale syn-flexural normal faults by comparing T-x and T-z profiles of various faults in two different seismic volumes along-strike the German Molasse. Furthermore, we also used syn-flexural normal fault activity to calculate the Oligocene continent-ward propagation of the orogen-forebulge system. The main conclusions of our study are as follows:

1. The observed fault network records deformation associated with both reactivation of Mesozoic faults and newly nucleated Cenozoic syn-flexural normal faults. Deformation was dominated by orogen-parallel E-W striking faults, dipping both N and S. Few of these faults are connected with shorter NW-SE striking relay faults.
2. The nucleation of syn-flexural normal faults at the onset of flexure occurs close to or at the surface of the foreland plate around the forebulge. This is because the magnitude

of extensional deformation is maximum along the hinge line at the surface of the forebulge, promoting the nucleation of new faults.

3. In cases where pre-existing faults were buried at greater depths (> 480 m) in the pre-flexural basement, they were not reactivated in the German Molasse. Instead, they may characterise a lower segment of a dip-linked fault.
4. The lateral fault growth of newly nucleated normal faults in the German Molasse followed either the isolated or hybrid fault growth model. In contrast, reactivated faults followed the constant-length growth model.
5. During lateral fault growth, fault tips of syn-flexural faults in the German Molasse migrated stratigraphically upward as fault planes grew laterally.
6. Spatiotemporal variations in the nucleation of normal fault activity in foreland basins can be used to calculate the migration rate of the orogen-forebulge system. Consistent with results from other independent methods, we find that the Alpine orogen-forebulge system migrated northward with an average velocity of 7.8 mm/year during the Oligocene.
7. The eastward increase in the cumulative offsets of the syn-flexural normal faults correlates with the lateral decrease and increase in strength of the European lithosphere and crust, respectively. This implies that lithospheric strength exerts a first-order control on foreland flexure. However, the contribution of along-strike variations in slab loads cannot be excluded.
8. The Oligocene to early Miocene orogen-parallel variations in sedimentary and topographic loading were not the primary mechanisms controlling the distribution of flexure in the German Molasse.
9. As suggested before by Willingshofer and Sokoutis (2009), we find that coupling between the Alps and the European plate increased during the early to middle Miocene, resulting in enhanced efficiency in compressional stress transfer into the German Molasse and, thereby, cessation of extensional normal faulting.
10. An eastward decrease in the strength of the European lithosphere contributed to the Oligocene to early Miocene increase in magnitude of deflection of the European plate to the east. Additionally, the Landshut-Neuoetting High and the Bohemian Massif (Andeweg and Cloetingh 1998) may have acted as buttresses in front of the approaching Alpine orogen, further enhancing the narrowing and deepening of the flexural profile to the east due to downward squeezing. This is reflected in higher syn-flexural offsets along the normal faults in a narrower band in the Eastern German Molasse compared to the Western German Molasse.

Acknowledgements

This study was supported by the Deutsche Forschungsgemeinschaft (DFG) grant to Nevena Andrić-Tomašević (TO 1364/1-1) within the priority programme 4D-MB and contributed to the AlpArray initiative. We thank SLB for providing an academic Petrel licence. Furthermore, we thank ONEO GmbH & Co. KG for providing us with the two seismic volumes presented in this study. We would like to thank Matthias Müller and Rolf Herrmann for the discussions that contributed to the content of this paper. We are grateful to E. Willingshofer and I. Moeck for their insightful and constructive suggestions for an earlier version of this manuscript. Lastly, the manuscript benefitted from discussions with Eline Le Breton (FU Berlin), Mark Handy (FU Berlin), Hugo Ortner (University of Innsbruck) and Vladimir Shipilin (Geological Survey of North Rhine-Westphalia). Open Access funding was enabled and organised by Projekt DEAL.

Conflicts of Interest

The authors declare no conflicts of interest.

Data Availability Statement

In this research, we used the software packages QGIS (version 3.2), Petrel (version 2021) and CorelDraw (version 2021) to interpret the seismic data, construct the geological model and create the figures presented in this paper. For the seismic data presented, open access does not apply, and ONEO GmbH should be contacted. The Python code, which was used to extract throw data from Petrel to calculate and generate backstripped throw-length and throw-depth profiles, is available for download on GitHub upon request.

References

Andeweg, B., and S. Cloetingh. 1998. "Flexure and 'Unflexure' of the North Alpine German-Austrian Molasse Basin: Constraints From Forward Tectonic Modelling." *Geological Society, London, Special Publications* 134, no. 1: 403–422.

Andrić-Tomašević, N., A. Koptev, G. Maiti, T. Gerya, and T. A. Ehlers. 2023. "Slab Tearing in Non-collisional Settings: Insights From Thermo-Mechanical Modelling of Oblique Subduction." *Earth and Planetary Science Letters* 610: 118097.

Bachmann, G. H., and M. Müller. 1991. "The Molasse Basin, Germany: Evolution of a Classic Petroliferous Foreland Basin. Generation, Accumulation, and Production of Europe's Hydrocarbons. Special Publication of the European Association of Petroleum Geoscientists." *European Association of Petroleum Geoscientists Special Publications* 1: 263–276.

Balázs, A., I. Magyar, L. Matenco, O. Sztanó, L. Tőkés, and F. Horváth. 2018. "Morphology of a Large Paleo-Lake: Analysis of Compaction in the Miocene-Quaternary Pannonian Basin." *Global and Planetary Change* 171: 134–147.

Baudon, C., and J. Cartwright. 2008. "Early Stage Evolution of Growth Faults: 3D Seismic Insights From the Levant Basin, Eastern Mediterranean." *Journal of Structural Geology* 30, no. 7: 888–898.

Beaumont, C. 1981. "Foreland Basins." *Geophysical Journal International* 65, no. 2: 291–329.

Bergerat, F. 1987. "Stress Fields in the European Platform at the Time of Africa-Eurasia Collision." *Tectonics* 6, no. 2: 99–132.

Bosworth, W. 1985. "Geometry of Propagating Continental Rifts." *Nature* 316, no. 6029: 625–627.

Bradley, D., and W. Kidd. 1991. "Flexural Extension of the Upper Continental Crust in Collisional Foredeeps." *Geological Society of America Bulletin* 103, no. 11: 1416–1438.

Brink, H.-J., P. Burri, A. Lunde, and H. Winhard. 1992. "Hydrocarbon Habitat and Potential of Swiss and German Molasse Basin: A Comparison." *Eclogae Geologicae Helvetiae* 85, no. 3: 715–732.

Bry, M., N. White, S. Singh, R. England, and C. Trowell. 2004. "Anatomy and Formation of Oblique Continental Collision: South Falkland Basin." *Tectonics* 23, no. 4: 1–20.

Budach, I., I. Moeck, E. Lüschen, and M. Wolfgramm. 2018. "Temporal Evolution of Fault Systems in the Upper Jurassic of the Central German Molasse Basin: Case Study Unterhaching." *International Journal of Earth Sciences* 107, no. 2: 635–653.

Burov, E. 2010. "The Equivalent Elastic Thickness (Te), seismicity and the Long-Term Rheology of Continental Lithosphere: Time to Burn-Out "crème brûlée"?: Insights From Large-Scale Geodynamic Modeling." *Tectonophysics* 484, no. 1–4: 4–26.

Calignano, E., D. Sokoutis, E. Willingshofer, F. Gueydan, and S. Cloetingh. 2015. "Strain Localization at the Margins of Strong Lithospheric Domains: Insights From Analog Models." *Tectonics* 34, no. 3: 396–412.

Cartwright, J. A., C. Mansfield, and B. Trudgill. 1996. "The Growth of Normal Faults by Segment Linkage." *Geological Society, London, Special Publications* 99, no. 1: 163–177.

Chapman, T., and A. Meneilly. 1991. "The Displacement Patterns Associated With a Reverse-Reactivated, Normal Growth Fault." *Geological Society, London, Special Publications* 56, no. 1: 183–191.

Cordero Peña, F. A. 2007. "The Early Miocene Upper Marine Molasse of the German Part of the Molasse Basin: A Subsurface Study; Sequence Stratigraphy, Depositional Environment and Architecture, 3D Basin Modeling." Tübingen, Univ., Diss.

Crampton, S., and P. Allen. 1995. "Recognition of Forebulge Unconformities Associated With Early Stage Foreland Basin Development: Example From the North Alpine Foreland Basin." *AAPG Bulletin* 79, no. 10: 1495–1514.

Davies, J. H., and F. von Blanckenburg. 1995. "Slab Breakoff: A Model of Lithosphere Detachment and Its Test in the Magmatism and Deformation of Collisional Orogens." *Earth and Planetary Science Letters* 129, no. 1–4: 85–102.

DeCelles, P. G. 2012. "Foreland Basin Systems Revisited: Variations in Response to Tectonic Settings." In *Tectonics of Sedimentary Basins: Recent Advances*, 405–426. Hoboken, NJ: Blackwell Publishing Ltd.

DeCelles, P. G., and K. A. Giles. 1996. "Foreland Basin Systems." *Basin Research* 8, no. 2: 105–123.

Diem, B. 1986. "Die Untere Meeresmolasse zwischen der Saane (Westschweiz) und der Ammer (Oberbayern)." *Eclogae Geologicae Helvetiae* 79, no. 2: 493–559.

Eizenhöfer, P. R., C. Glotzbach, J. Kley, and T. A. Ehlers. 2023. "Thermo-Kinematic Evolution of the Eastern European Alps Along the TRANSALP Transect." *Tectonics* 42: e2022TC007380.

Eskens, L. H., N. Andrić-Tomašević, P. M. Süss, M. Müller, R. Herrmann, and T. A. Ehlers. 2024. "Lithospheric-and Crustal-Scale Controls on Variations in Foreland Basin Development in the Northern Alpine Foreland Basin." *Tectonophysics* 878: 230283.

Faupl, P., and M. Wagreich. 2000. "Late Jurassic to Eocene Palaeogeography and Geodynamic Evolution of the Eastern Alps." *Mitteilungen der Österreichischen Geologischen Gesellschaft* 92, no. 1999: 79–94.

Favaro, S., R. Schuster, M. R. Handy, A. Scharf, and G. Pestal. 2015. "Transition From Orogen-Perpendicular to Orogen-Parallel Exhumation and Cooling During Crustal Indentation—Key Constraints From $^{147}Sm/^{144}Nd$ and 87Rb/87Sr Geochronology (Tauern Window, Alps)." *Tectonophysics* 665: 1–16.

Flemings, P. B., and T. E. Jordan. 1989. "A Synthetic Stratigraphic Model of Foreland Basin Development." *Journal of Geophysical Research: Solid Earth* 94, no. B4: 3851–3866.

Flemings, P. B., and T. E. Jordan. 1990. "Stratigraphic Modeling of Foreland Basins: Interpreting Thrust Deformation and Lithosphere Rheology." *Geology* 18, no. 5: 430–434.

Fomel, S., and E. Landa. 2014. "Structural Uncertainty of Time-Migrated Seismic Images." *Journal of Applied Geophysics* 101: 27–30.

Fosdick, J. C., S. A. Graham, and G. E. Hilley. 2014. "Influence of Attenuated Lithosphere and Sediment Loading on Flexure of the Deep-Water Magallanes Retroarc Foreland Basin, Southern Andes." *Tectonics* 33, no. 12: 2505–2525.

Fox, M., F. Herman, S. D. Willett, and S. M. Schmid. 2016. "The Exhumation History of the European Alps Inferred From Linear Inversion of Thermochronometric Data." *American Journal of Science* 316, no. 6: 505–541.

Freudenberger, W., and K. Schwerd. 1996. "Erläuterungen zur Geologischen Karte von Bayern 1: 500000.-4 Aufl., 329 S., 67 Abb., 21 Tab., 8 Beil." München (GLA).

Frisch, W., J. Kuhlemann, I. Dunkl, and B. Székely. 2001. "The Dachstein Paleosurface and the Augenstein Formation in the Northern Calcareous Alps–A Mosaic Stone in the Geomorphological Evolution of the Eastern Alps." *International Journal of Earth Sciences* 90: 500–518.

Gawthorpe, R. L., C. A.-L. Jackson, M. J. Young, I. R. Sharp, A. R. Moustafa, and C. W. Leppard. 2003. "Normal Fault Growth, Displacement Localisation and the Evolution of Normal Fault Populations: The Hammam Faraun Fault Block, Suez Rift, Egypt." *Journal of Structural Geology* 25, no. 6: 883–895.

Giba, M., A. Nicol, and J. Walsh. 2010. "Evolution of Faulting and Volcanism in a Back-Arc Basin and Its Implications for Subduction Processes." *Tectonics* 29, no. 4: 1–18.

Giba, M., J. Walsh, and A. Nicol. 2012. "Segmentation and Growth of an Obliquely Reactivated Normal Fault." *Journal of Structural Geology* 39: 253–267.

Gross, D., R. Sachsenhofer, A. Rech, et al. 2015. "The Trattnach Oil Field in the North Alpine Foreland Basin (Austria)." *Austrian Journal of Earth Sciences* 108, no. 2: 151–171.

Handy, M. R., S. M. Schmid, R. Bousquet, E. Kissling, and D. Bernoulli. 2010. "Reconciling Plate-Tectonic Reconstructions of Alpine Tethys With the Geological–Geophysical Record of Spreading and Subduction in the Alps." *Earth-Science Reviews* 102, no. 3–4: 121–158.

Handy, M. R., K. Ustaszewski, and E. Kissling. 2015. "Reconstructing the Alps–Carpathians–Dinarides as a Key to Understanding Switches in Subduction Polarity, Slab Gaps and Surface Motion." *International Journal of Earth Sciences* 104, no. 1: 1–26.

Heckeberg, N., M. Pippèrr, B. Läuchli, F. U. Heimann, and B. Reichenbacher. 2010. "The Upper Marine Molasse (Burdigalian, Ottnangian) in Southwest Germany-Facies Interpretation and a New Lithostratigraphic Terminology." *Zeitschrift der Deutschen Gesellschaft Fur Geowissenschaften* 161, no. 3: 285–302.

Heimann, F. U., D. U. Schmid, M. Pipperr, and B. Reichenbacher. 2009. "Re-Interpreting the Baltringer Horizont as a Subtidal Channel Facies: Implications for a New Understanding of the Upper Marine Molasse "Cycles" (Early Miocene)." *Neues Jahrbuch Fur Geologie Und Palaontologie-Abhandlungen* 254, no. 1: 135–149.

Hempton, M. R., and L. A. Dunne. 1984. "Sedimentation in Pull-Apart Basins: Active Examples in Eastern Turkey." *Journal of Geology* 92, no. 5: 513–530.

Heuberger, S., P. Roth, O. Zingg, H. Naef, and B. P. Meier. 2016. "The St. Gallen Fault Zone: A Long-Lived, Multiphase Structure in the North Alpine Foreland Basin Revealed by 3D Seismic Data." *Swiss Journal of Geosciences* 109, no. 1: 83–102.

Hinsch, R. 2013. "Laterally Varying Structure and Kinematics of the Molasse Fold and Thrust Belt of the Central Eastern Alps: Implications for Exploration." *AAPG Bulletin* 97, no. 10: 1805–1831.

Hongxing, G., and J. K. Anderson. 2007. "Fault Throw Profile and Kinematics of Normal Fault: Conceptual Models and Geologic Examples." *Geological Journal of China Universities* 13, no. 1: 75.

Hülscher, J., G. Fischer, P. Grunert, G. Auer, and A. Bernhardt. 2019. "Selective Recording of Tectonic Forcings in an Oligocene/Miocene Submarine Channel System: Insights From New Age Constraints and Sediment Volumes From the Austrian Northern Alpine Foreland Basin." *Frontiers in Earth Science* 7, no. 302: 1–25.

Hurford, A. J. 1986. "Cooling and Uplift Patterns in the Lepontine Alps South Central Switzerland and an Age of Vertical Movement on the Insubric Fault Line." *Contributions to Mineralogy and Petrology* 92, no. 4: 413–427.

Jackson, C. A.-L., R. E. Bell, A. Rotevatn, and A. B. Tvedt. 2017. "Techniques to Determine the Kinematics of Synsedimentary Normal Faults and Implications for Fault Growth Models." *Geological Society, London, Special Publications* 439, no. 1: 187–217.

Jackson, C. A.-L., and A. Rotevatn. 2013. "3D Seismic Analysis of the Structure and Evolution of a Salt-Influenced Normal Fault Zone: A Test of Competing Fault Growth Models." *Journal of Structural Geology* 54: 215–234.

Jácome, M. I., N. Kusznir, F. Audemard, and S. Flint. 2003. "Formation of the Maturin Foreland Basin, Eastern Venezuela: Thrust Sheet Loading or Subduction Dynamic Topography." *Tectonics* 22, no. 5: 1–17.

Jin, J., T. Aigner, H. Luterbacher, G. H. Bachmann, and M. Müller. 1995. "Sequence Stratigraphy and Depositional History in the South-Eastern German Molasse Basin." *Marine and Petroleum Geology* 12, no. 8: 929–940.

Koson, S., P. Chenrai, and M. Choowong. 2013. "Seismic Attributes and Their Applications in Seismic Geomorphology." *Bulletin of Earth Sciences of Thailand* 6, no. 1: 1–9.

Krsnik, E., K. Methner, M. Campani, et al. 2021. "Miocene High Elevation in the Central Alps." *Solid Earth* 12, no. 11: 2615–2631.

Krzywiec, P. 2001. "Contrasting Tectonic and Sedimentary History of the Central and Eastern Parts of the Polish Carpathian Foredeep Basin—Results of Seismic Data Interpretation." *Marine and Petroleum Geology* 18, no. 1: 13–38.

Kuhlemann, J. 2007. "Paleogeographic and Paleotopographic Evolution of the Swiss and Eastern Alps Since the Oligocene." *Global and Planetary Change* 58, no. 1–4: 224–236.

Kuhlemann, J., and O. Kempf. 2002. "Post-Eocene Evolution of the North Alpine Foreland Basin and Its Response to Alpine Tectonics." *Sedimentary Geology* 152, no. 1–2: 45–78.

La Bruna, V., F. Agosta, J. Lamarche, S. Viseur, and G. Prosser. 2018. "Fault Growth Mechanisms and Scaling Properties in Foreland Basin System: The Case Study of Monte Alpi, Southern Apennines, Italy." *Journal of Structural Geology* 116: 94–113.

Langhi, L., N. B. Ciftci, and G. D. Borel. 2011. "Impact of Lithospheric Flexure on the Evolution of Shallow Faults in the Timor Foreland System." *Marine Geology* 284, no. 1–4: 40–54.

Lash, G. G. 1988. "Along-Strike Variations in Foreland Basin Evolution: Possible Evidence for Continental Collision Along an Irregular Margin." *Basin Research* 1, no. 2: 71–83.

Le Breton, E., S. Brune, K. Ustaszewski, S. Zahirovic, M. Seton, and R. D. Müller. 2021. "Kinematics and Extent of the Piemont–Liguria Basin–Implications for Subduction Processes in the Alps." *Solid Earth* 12, no. 4: 885–913.

Lemcke, K. 1987. "Zur Frage der alten Verkarstung des Malm im Untergrund des deutschen Molassebeckens und an dessen Nordwestrand." *Bulletin der Vereinigung Schweizerischer Petroleum-Geologen Und-Ingenieure* 53, no. 125: 33–46.

Lemcke, K. 1988. "Das bayerische Alpenvorland vor der Eiszeit."

Maiti, G., A. Koptev, P. Baville, T. Gerya, S. Crosetto, and N. Andrić-Tomašević. 2024. "Topography Response to Horizontal Slab Tearing and Oblique Continental Collision: Insights From 3D Thermomechanical Modeling." *Journal of Geophysical Research: Solid Earth* 129, no. 10: e2024JB029385.

Mann, P., M. R. Hempton, D. C. Bradley, and K. Burke. 1983. "Development of Pull-Apart Basins." *Journal of Geology* 91, no. 5: 529–554.

Masalimova, L. U., D. R. Lowe, T. Mchargue, and R. Derksen. 2015. "Interplay Between an Axial Channel Belt, Slope Gullies and Overbank Deposition in the Puchkirchen Formation in the Molasse Basin, Austria." *Sedimentology* 62, no. 6: 1717–1748.

Maţenco, L., R. Zoetemeijer, S. Cloetingh, and C. Dinu. 1997. "Lateral Variations in Mechanical Properties of the Romanian External Carpathians: Inferences of Flexure and Gravity Modelling." *Tectonophysics* 282, no. 1–4: 147–166.

Matter, A. 1980. *Flysch and Molasse of Western and Central Switzerland*. Basel, Switzerland: Wepf & Co.

Meulenkamp, J., M. Kováč, and I. Cicha. 1996. "On Late Oligocene to Pliocene Depocentre Migrations and the Evolution of the Carpathian-Pannonian System." *Tectonophysics* 266, no. 1–4: 301–317.

Meyer, R. K., and H. Schmidt-Kaler. 1990a. "Paläogeographie und Schwammriffentwicklung des süddeutschen Malm—ein Überblick." *Facies* 23, no. 1: 175–184.

Meyer, R. K., and H. Schmidt-Kaler. 1990b. "Paläogeographischer Atlas des süddeutschen Oberjura (Malm)."

Mohn, G., G. Manatschal, M. Beltrando, and I. Haupert. 2014. "The Role of Rift-Inherited Hyper-Extension in Alpine-Type Orogens." *Terra Nova* 26, no. 5: 347–353.

Mraz, E., I. Moeck, S. Bissmann, and S. Hild. 2018. "Multiphase Fossil Normal Faults as Geothermal Exploration Targets in the Western Bavarian Molasse Basin: Case Study Mauerstetten." *Zeitschrift der Deutschen Gesellschaft für Geowissenschaften* 169, no. 3: 389–411.

Müller, M., F. Nieberding, and A. Wanninger. 1988. "Tectonic Style and Pressure Distribution at the Northern Margin of the Alps Between Lake Constance and the River Inn." *Geologische Rundschau* 77: 787–796.

Nanda, N. C. 2021. *Seismic Data Interpretation and Evaluation for Hydrocarbon Exploration and Production*. Cham: Springer.

Narkiewicz, M., A. Maksym, M. Malinowski, et al. 2015. "Transcurrent Nature of the Teisseyre–Tornquist Zone in Central Europe: Results of the POLCRUST-01 Deep Reflection Seismic Profile." *International Journal of Earth Sciences* 104: 775–796.

Ortner, H., S. Aichholzer, M. Zerlauth, R. Pilser, and B. Fügenschuh. 2015. "Geometry, Amount, and Sequence of Thrusting in the Subalpine Molasse of Western Austria and Southern Germany, European Alps." *Tectonics* 34, no. 1: 1–30.

Ortner, H., C. von Hagke, A. Sommaruga, et al. 2023. "The Northern Deformation Front of the European Alps." In *Geodynamics of the Alps 3: Collisional Processes*, edited by C. L. Rosenberg and N. Bellahsen, 241–312. London: ISTE-Wiley.

Pan, S., R. E. Bell, C. A. L. Jackson, and J. Naliboff. 2022. "Evolution of Normal Fault Displacement and Length as Continental Lithosphere Stretches." *Basin Research* 34, no. 1: 121–140.

Peacock, D., and D. Sanderson. 1991. "Displacements, Segment Linkage and Relay Ramps in Normal Fault Zones." *Journal of Structural Geology* 13, no. 6: 721–733.

Petersen, K., O. Clausen, and J. Korstgård. 1992. "Evolution of a Salt-Related Listric Growth Fault Near the D-1 Well, Block 5605, Danish North Sea: Displacement History and Salt Kinematics." *Journal of Structural Geology* 14, no. 5: 565–577.

Pfiffner, O. A. 1993. "The Structure of the Helvetic Nappes and Its Relation to the Mechanical Stratigraphy." *Journal of Structural Geology* 15, no. 3–5: 511–521.

Pfiffner, O.-A., F. Schlunegger, and S. Buiter. 2002. "The Swiss Alps and Their Peripheral Foreland Basin: Stratigraphic Response to Deep Crustal Processes." *Tectonics* 21, no. 2: 3-1-3-16.

Rankey, E., and J. Mitchell. 2003. "That's Why it's Called Interpretation: Impact of Horizon Uncertainty on Seismic Attribute Analysis." *Leading Edge* 22, no. 9: 820–828.

Ring, U., J. Glodny, T. Will, and S. Thomson. 2010. "The Hellenic Subduction System: High-Pressure Metamorphism, Exhumation, Normal Faulting, and Large-Scale Extension." *Annual Review of Earth and Planetary Sciences* 38: 45–76.

Roche, V., C. Childs, H. Madritsch, and G. Camanni. 2020. "Layering and Structural Inheritance Controls on Fault Zone Structure in Three Dimensions: A Case Study From the Northern Molasse Basin, Switzerland." *Journal of the Geological Society* 177, no. 3: 493–508.

Rosenberg, C. L., N. Bellahsen, A. Rabaute, and J. B. Girault. 2021. "Distribution, Style, Amount of Collisional Shortening, and Their Link to Barrovian Metamorphism in the European Alps." *Earth-Science Reviews* 222: 103774.

Rosenberg, C. L., and E. Kissling. 2013. "Three-Dimensional Insight Into Central-Alpine Collision: Lower-Plate or Upper-Plate Indentation?" *Geology* 41, no. 12: 1219–1222.

Rosenberg, C. L., S. Schneider, A. Scharf, et al. 2018. "Relating Collisional Kinematics to Exhumation Processes in the Eastern Alps." *Earth-Science Reviews* 176: 311–344.

Rotevatn, A., T. B. Kristensen, A. K. Ksienzyk, et al. 2018. "Structural Inheritance and Rapid Rift-Length Establishment in a Multiphase Rift: The East Greenland Rift System and Its Caledonian Orogenic Ancestry." *Tectonics* 37, no. 6: 1858–1875.

Roure, F. 2008. "Foreland and Hinterland Basins: What Controls Their Evolution?" *Swiss Journal of Geosciences* 101, no. 1: 5–29.

Rowan, M. G., B. S. Hart, S. Nelson, P. B. Flemings, and B. D. Trudgill. 1998. "Three-Dimensional Geometry and Evolution of a Salt-Related Growth-Fault Array: Eugene Island 330 Field, Offshore Louisiana, Gulf of Mexico." *Marine and Petroleum Geology* 15, no. 4: 309–328.

Ryan, L., C. Magee, and C. A.-L. Jackson. 2017. "The Kinematics of Normal Faults in the Ceduna Subbasin, Offshore Southern Australia: Implications for Hydrocarbon Trapping in a Frontier Basin." *AAPG Bulletin* 101, no. 3: 321–341.

Scharf, A., M. Handy, S. Favaro, S. M. Schmid, and A. Bertrand. 2013. "Modes of Orogen-Parallel Stretching and Extensional Exhumation in Response to Microplate Indentation and Roll-Back Subduction (Tauern Window, Eastern Alps)." *International Journal of Earth Sciences* 102, no. 6: 1627–1654.

Schlunegger, F., and E. Kissling. 2015. "Slab Rollback Orogeny in the Alps and Evolution of the Swiss Molasse Basin." *Nature Communications* 6, no. 1: 1–10.

Schlunegger, F., and E. Kissling. 2022. "Slab Load Controls Beneath the Alps on the Source-To-Sink Sedimentary Pathways in the Molasse Basin." *Geosciences* 12, no. 6: 226.

Schlunegger, F., and S. Willett. 1999. "Spatial and Temporal Variations in Exhumation of the Central Swiss Alps and Implications for Exhumation Mechanisms." *Geological Society, London, Special Publications* 154, no. 1: 157–179.

Schmid, S., B. Fügenschuh, E. Kissling, and R. Schuster. 2004. "TRANSMED Transects IV, V and VI: Three Lithospheric Transects Across the Alps and Their Forelands." In *The TRANSMED Atlas: The Mediterranean Region from Crust to Mantle*. Berlin, Germany: Springer Verlag.

Schmid, S. M., O.-A. Pfiffner, N. Froitzheim, G. Schönborn, and E. Kissling. 1996. "Geophysical-Geological Transect and Tectonic Evolution of the Swiss-Italian Alps." *Tectonics* 15, no. 5: 1036–1064.

Schmid, S. M., A. Scharf, M. R. Handy, and C. L. Rosenberg. 2013. "The Tauern Window (Eastern Alps, Austria): A New Tectonic Map, With Cross-Sections and a Tectonometamorphic Synthesis." *Swiss Journal of Geosciences* 106, no. 1: 1–32.

Scholz, C. H., and J. C. Contreras. 1998. "Mechanics of Continental Rift Architecture." *Geology* 26, no. 11: 967–970.

Shipilin, V., D. C. Tanner, H. von Hartmann, and I. Moeck. 2020. "Multiphase, Decoupled Faulting in the Southern German Molasse Basin–Evidence From 3-D Seismic Data." *Solid Earth* 11, no. 6: 2097–2117.

Sinclair, H. 1997a. "Flysch to Molasse Transition in Peripheral Foreland Basins: The Role of the Passive Margin Versus Slab Breakoff." *Geology* 25, no. 12: 1123–1126.

Sinclair, H. 1997b. "Tectonostratigraphic Model for Underfilled Peripheral Foreland Basins: An Alpine Perspective." *Geological Society of America Bulletin* 109, no. 3: 324–346.

Sissingh, W. 1997. "Tectonostratigraphy of the North Alpine Foreland Basin: Correlation of Tertiary Depositional Cycles and Orogenic Phases." *Tectonophysics* 282, no. 1–4: 223–256.

Smit, J., J.-D. V. Wees, and S. Cloetingh. 2016. "The Thor Suture Zone: From Subduction to Intraplate Basin Setting." *Geology* 44, no. 9: 707–710.

Spooner, C., M. Scheck-Wenderoth, M. Cacace, and D. Anikiev. 2022. "How Alpine Seismicity Relates to Lithospheric Strength." *Solid Earth Discussions* 2020: 1–24.

Stampfli, G., J. Mosar, D. Marquer, R. Marchant, T. Baudin, and G. Borel. 1998. "Subduction and Obduction Processes in the Swiss Alps." *Tectonophysics* 296, no. 1–2: 159–204.

Subrahmanyam, D., and P. Rao. 2008. "Seismic Attributes-A Review." 7th International Conference & Exposition on Petroleum Geophysics, Hyderabad, pp. 398–404.

Supak, S., D. Bohnenstiehl, and W. Buck. 2006. "Flexing Is Not Stretching: An Analogue Study of Flexure-Induced Fault Populations." *Earth and Planetary Science Letters* 246, no. 1–2: 125–137.

Thorsen, C. E. 1963. "Age of Growth Faulting in Southeast Louisiana."

Trümpy, R. 1960. "Paleotectonic Evolution of the Central and Western Alps." *Geological Society of America Bulletin* 71, no. 6: 843–907.

Van Hinsbergen, D. J., T. H. Torsvik, S. M. Schmid, et al. 2020. "Orogenic Architecture of the Mediterranean Region and Kinematic Reconstruction of Its Tectonic Evolution Since the Triassic." *Gondwana Research* 81: 79–229.

von Hartmann, H., D. C. Tanner, and S. Schumacher. 2016. "Initiation and Development of Normal Faults Within the German Alpine Foreland Basin: The Inconspicuous Role of Basement Structures." *Tectonics* 35, no. 6: 1560–1574.

Walsh, J., W. Bailey, C. Childs, A. Nicol, and C. Bonson. 2003. "Formation of Segmented Normal Faults: A 3-D Perspective." *Journal of Structural Geology* 25, no. 8: 1251–1262.

Walsh, J., A. Nicol, and C. Childs. 2002. "An Alternative Model for the Growth of Faults." *Journal of Structural Geology* 24, no. 11: 1669–1675.

Wang, S., K. Liu, H. Wang, and M. Chen. 2022. "Growth and Linkage of Normal Faults Experiencing Multiple Non-coaxial Extension: A Case From the Qikou Sag, Bohai Bay Basin, East China." *Basin Research* 34, no. 2: 748–770.

Waschbusch, P. J., and L. H. Royden. 1992. "Spatial and Temporal Evolution of Foredeep Basins: Lateral Strength Variations and Inelastic Yielding in Continental Lithosphere." *Basin Research* 4, no. 3–4: 179–196.

Watts, A., and E. Burov. 2003. "Lithospheric Strength and Its Relationship to the Elastic and Seismogenic Layer Thickness." *Earth and Planetary Science Letters* 213, no. 1–2: 113–131.

Whipp, P., C. L. Jackson, R. Gawthorpe, T. Dreyer, and D. Quinn. 2014. "Normal Fault Array Evolution Above a Reactivated Rift Fabric; a Subsurface Example From the Northern Horda Platform, Norwegian North Sea." *Basin Research* 26, no. 4: 523–549.

Willingshofer, E., and S. Cloetingh. 2003. "Present-Day Lithospheric Strength of the Eastern Alps and Its Relationship to Neotectonics." *Tectonics* 22, no. 6: 1–14.

Willingshofer, E., and D. Sokoutis. 2009. "Decoupling Along Plate Boundaries: Key Variable Controlling the Mode of Deformation and the Geometry of Collisional Mountain Belts." *Geology* 37, no. 1: 39–42.

Willingshofer, E., D. Sokoutis, and J.-P. Burg. 2005. "Lithospheric-Scale Analogue Modelling of Collision Zones With a Pre-Existing Weak Zone." *Geological Society, London, Special Publications* 243, no. 1: 277–294.

Wolpert, P., T. Aigner, D. Bendias, K. Beichel, and K. Zosseder. 2022. "A Novel Workflow for Geothermal Exploration: 3D Seismic Interpretation of Biohermal Buildups (Upper Jurassic, Molasse Basin, Germany)." *Geothermal Energy* 10, no. 1: 1–20.

Ziegler, P., G. Bertotti, and S. Cloetingh. 2002. "Dynamic Processes Controlling Foreland Development–The Role of Mechanical (de) Coupling of Orogenic Wedges and Forelands." *EGU Stephan Mueller Special Publication Series* 1: 17–56.

Ziegler, P. A. 1990. *Geological Atlas of Western and Central Europe, 1*. London, UK: Geological Society Publishing House.

Ziegler, P. A., S. Schmid, A. Pfiffner, and G. Schönborn. 1996. "Structure and Evolution of the Central Alps and Their Northern and Southern Foreland Basins." *Mémoires du Muséum national d'histoire Naturelle* 1993, no. 170: 211–233.

Zweigel, J., T. Aigner, and H. Luterbacher. 1998. "Eustatic Versus Tectonic Controls on Alpine Foreland Basin Fill: Sequence Stratigraphy and Subsidence Analysis in the SE German Molasse." *Geological Society, London, Special Publications* 134, no. 1: 299–323.

von Doppler, G., K. Heissig, and B. Reichenbacher. 2005. "Die Gliederung des Tertiärs im süddeutschen Molassebecken." *Newsletters on Stratigraphy* 41: 359–375.

Zhang, J., H. Yang, G. Zhu, H. Chen, F. Zhang, and Z. Sun. 2023. "The Effect of Along-Strike Variable Plate Deflection on Bending Stress and Seismicity at the Southern Mariana Trench." *Tectonophysics* 850: 229752.

Supporting Information

Additional supporting information can be found online in the Supporting Information section.

Appendix A

Seismic Data, Horizon Tracing and Fault Interpretations

Seismic volumes A and B are located in the Western and Eastern German Molasse, respectively (Figure 1 for locations). Seismic volume A is an APSDM (anisotropic pre-stack depth migrated) seismic volume in the depth domain, which images down to a depth of 2000 m and covers an area of 145 km^2. Seismic Volume B is a PreSTM (pre-stack time migrated) seismic volume that covers an area of 560 km^2. It images down to a 5000 ms TWTT depth, with the upper 2500 ms TWTT being of interpretable quality. The line spacing for both seismic volumes is 25 m. For the fault analysis, seismic volume B was converted from the time to the depth domain (see Section A2 for specifics on the time to depth conversion). Based on the dominant frequency of 45 Hz in volume B and the average velocity of 2678 m/s in the stratigraphic sequence of interest (Section A2), the vertical resolution is up to 15 m ($\lambda/4$; Nanda 2021). Furthermore, both seismic volumes are displayed in reverse polarity (SEG convention). This means that a blue reflector (negative amplitude) indicates a downward increase in acoustic impedance. In contrast, a red reflector (positive amplitude) characterises a downward decrease in acoustic impedance.

The structural smoothing seismic attribute was applied to the input seismic data to increase the signal-to-noise ratio for the conventional tracing of prominent seismic horizons. Key stratigraphic horizons were identified based on well data. In seismic volume A, eight different reflectors were mapped, from oldest to youngest: top Lias, top Dogger, base karstified Upper Jurassic limestones, top Upper Jurassic limestones (i.e., foreland unconformity in this volume), top Baustein Beds, top Cyrena Beds, top Lower Freshwater Molasse (*Untere Süßwassermolasse*, USM) and top Baltringer Formation (Fm.) (Figure 3). Because the top USM reflector is very discontinuous in seismic volume A, the USM deposits above the Cyrena Beds and the Early Burdigalian reflectors until the top Baltringer reflector were considered as a single seismic-stratigraphic unit. In seismic volume B, seven seismic horizons have been mapped: top Turonian, base Eocene (i.e., foreland unconformity), top Eocene, top Rupelian, top Chattian Sands, Base Hall Formation and top Hall Formation. Fault interpretations were based on lateral reflector terminations (i.e., juxtaposing different seismic facies or contrasting amplitudes). Furthermore, the variance seismic attribute (Subrahmanyam and Rao 2008; Koson, Chenrai, and Choowong 2013) was applied to the structurally smoothened seismic data to further enhance the confidence in the fault interpretation as well as to highlight sedimentary structures.

Time to Depth Conversion of Seismic Volume B

Fault throw in time-domain seismic datasets may not necessarily correctly reflect discrepancies in throw values for different reflectors. Therefore, the seismic data from volume B must be converted from the time to the depth domain. Initially, reflectors were picked in the time domain based on well data where checkshot data are available. Based on this same well data, the true depth of the reflectors is also known in meters, allowing for the calculation of an average velocity from the surface to the depth of the reflector. This was done for every reflector that could be traced through the entire seismic volume and had corresponding well top data (Table A1). Based on the average velocities of the separate horizons, the average velocity for the entire stratigraphic sequence is 2678 m/s. This velocity was used to convert the seismic data from the time to the depth domain. Subsequently, reflectors and faults were then picked on the depth-converted seismic data. These interpretations were then used as input for structural modelling in Petrel to derive throw values for each horizon of interest along all the faults in each seismic volume.

Cumulative Cenozoic Offsets Along Syn-Flexural Normal Faults: From Milliseconds to Meters

Taking the seismic interpretation of Line I from (Cordero Peña 2007), the foreland unconformity has a throw value of 186 ms TWT. At the location of well '5 Ost' along this seismic line (Cordero Peña 2007, their figure 36), the foreland unconformity is located at a depth of 2221 ms TWT. As well '5 Ost' represents the Bromberg-1 well, we also know

TABLE A1 | Average velocities from the surface to interpreted seismic horizon.

Stratigraphic surface	Average velocity (m/s)	Number of wells
Base Hall unconformity	2709	93
Top Chattian Sands	2516	91
Base Eocene	2729	63
Top Turonian	2739	10

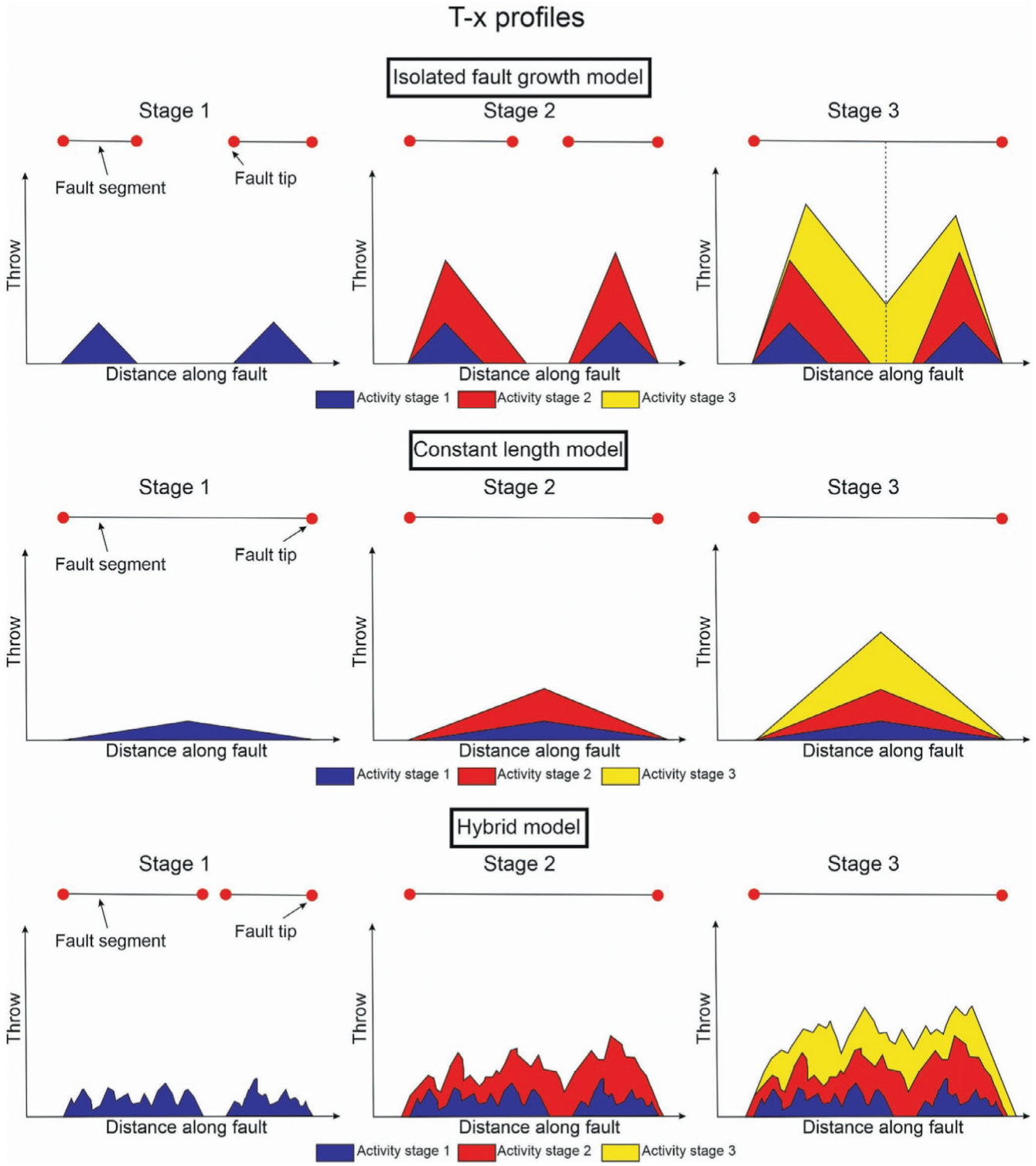

FIGURE A1 | Conceptual model for lateral (along-strike) normal fault growth signature in T-x graphs for the isolated, constant length and hybrid fault growth models. For the isolated fault growth model, lateral growth occurs through tip migration and subsequent linkage of initially separated fault segments. Modified from Peacock and Sanderson (1991), Hongxing and Anderson (2007), Ryan, Magee, and Jackson (2017) and Wang et al. (2022). For the constant length model, the final length of the fault is established during the early stages of fault development, accumulating offset along the entire fault over time (Walsh, Nicol, and Childs 2002; Jackson and Rotevatn 2013; Jackson et al. 2017). The hybrid model combines the isolated and constant-length growth models. In this case, the early stage is defined by the lengthening of the fault, laterally linking along (most of) its length. Subsequently, offset accumulates along the fault coeval with minor lengthening (Jackson et al. 2017).

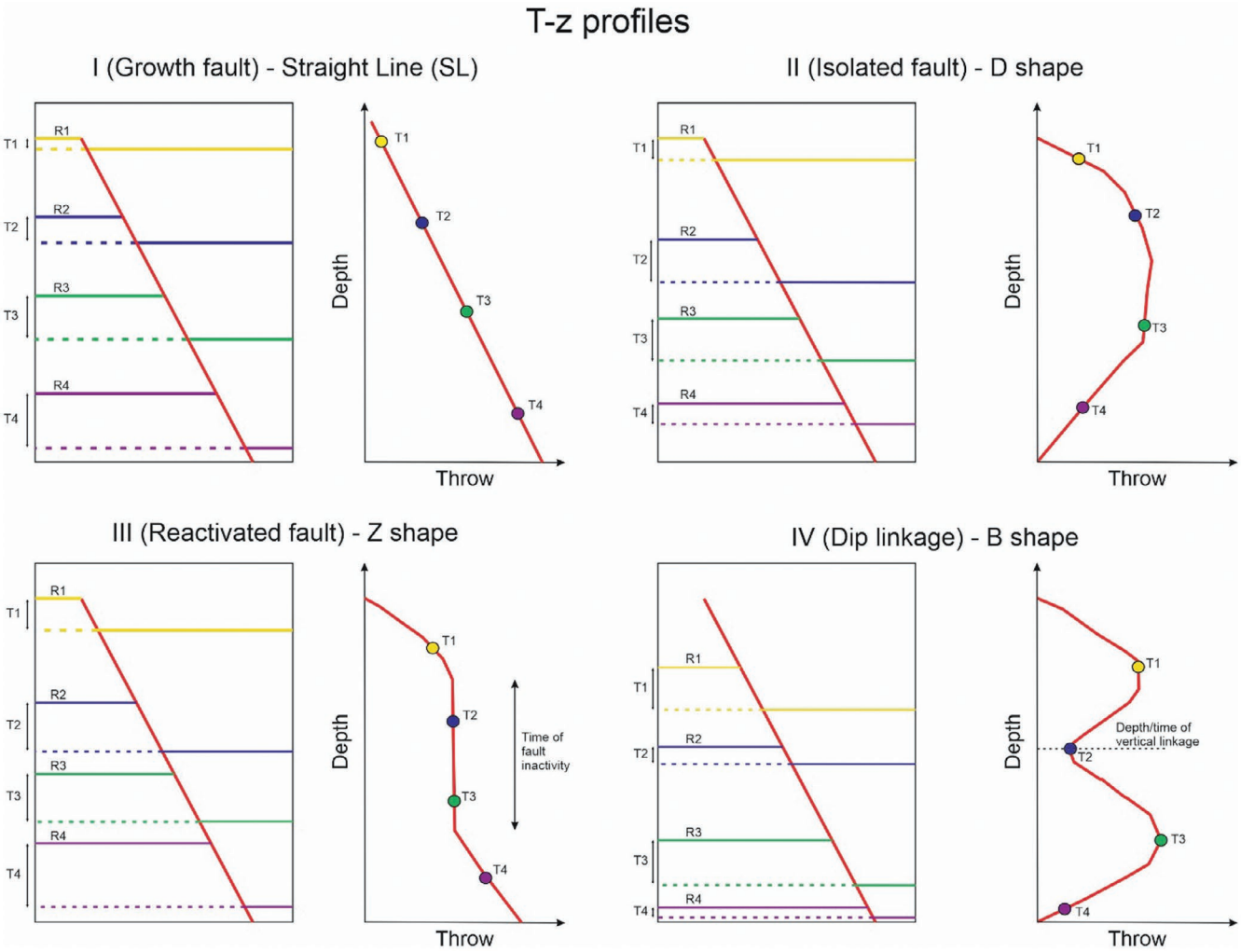

FIGURE A2 | Conceptual models for down-dip (vertical) normal fault growth signature in T-z graphs. Assuming the entire fault surface is active during phases of tectonic activity, the stratigraphic surface that records the highest offset indicates the time and point of initial nucleation. (I) A growth fault nucleates at depth, growing continuously upward in the stratigraphy. In a T-z graph, this is recognised as an upward continuous decrease in offsets compared to the lowest stratigraphic surface (Hongxing and Anderson 2007; Ryan, Magee, and Jackson 2017). (II) An isolated fault nucleates in the middle of a stratigraphic sequence, subsequently propagating both downward and upward in the stratigraphy. This is recognised in a T-z graph as the highest offset being recorded midway down the fault, decreasing both downward and upward (Hongxing and Anderson 2007), giving the T-z profile a D-shape. (III) A reactivated fault nucleates at depth, subsequently becoming inactive before being reactivated during a second phase of activity. In a T-z graph, this is recognised as the maximum throws being observed for the deepest stratigraphic surface, remaining constant for a few surfaces before subsequently decreasing for the youngest stratigraphy cut by the fault (Ryan, Magee, and Jackson 2017), giving the T-z profile a Z-shape. (IV) A vertically dip-linked fault initially consisted of two mechanically separated segments that link as both faults grew downward and upward. In a T-z graph, this is reflected by two throw maxima at different depths with decreasing offsets both downward and upward. Between the throw maxima, a throw minimum indicates the vertical linkage position (Baudon and Cartwright 2008). Overall, this gives the T-z profile a B-shape. Modified from Wang et al. (2022).

the foreland unconformity is located at a depth of 3622 m (Müller, Nieberding, and Wanninger 1988, their figure 10). Taken together, this gives an estimate of 3260 m/s for the average seismic velocity of the sediments up until the foreland unconformity. Therefore, the 186 ms offset of the foreland unconformity in the time domain corresponds to an offset of 303 m in the depth domain.

Limitations and Pitfalls of Structural Analyses Based on Seismic Data

Structural information in the time-migrated seismic volume B and time-migrated data presented by previous authors is inherently uncertain (e.g., Fomel and Landa 2014). Moreover, uncertainties in the applied velocity model to convert this volume to the depth domain are passed along to the constructed T-x and T-z profiles. With a seismic resolution of up to 15 m (Section A.1), shifting the pick of an interpreted horizon to a single reflector higher or lower in the seismic data can drastically change the geometry of the T-z profiles, backstripped T-x profiles or seismic attributes used to constrain structures (Rankey and Mitchell 2003). As a result, the structural history as interpreted from the T-z and backstripped T-x profiles in seismic volume B are more uncertain compared to those from seismic volume A. Lastly, as outlined in the methodology section, seismic data do not allow for the quantitative determination of the dip- and oblique-slip components for the normal faults. However, the lack of throw maxima migrating along the faults in the T-x profiles may indicate that oblique slip was negligible.

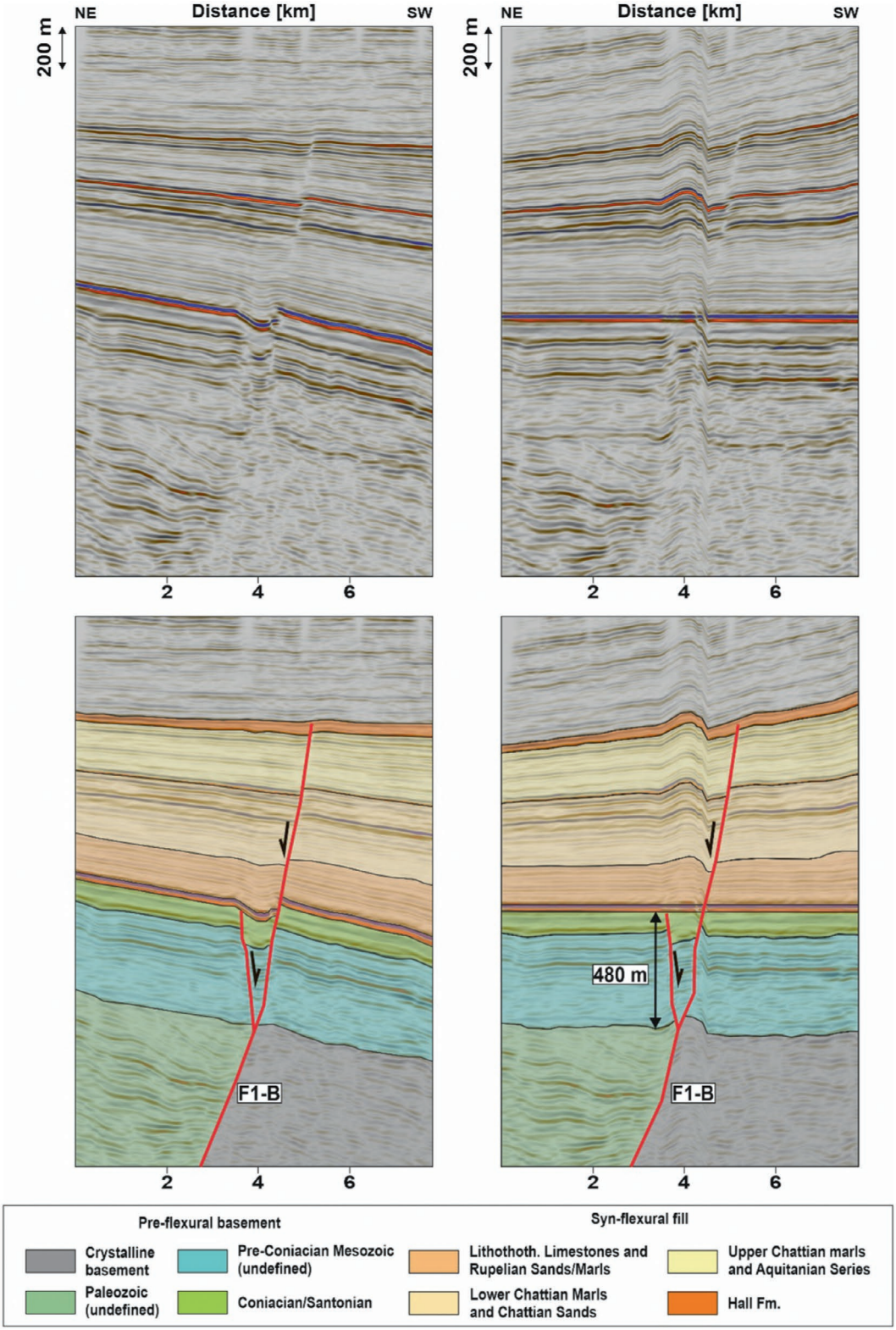

FIGURE A3 | Left panels show both an uninterpreted and interpreted unflattened section across F1-B. Right panels show both an uninterpreted and interpreted version of the same section, flattened on the foreland unconformity reflector. This section indicates that at the onset of flexure, the lower segment of F1-B, which was not reactivated during flexure, was buried at a depth of approximately 480 m.

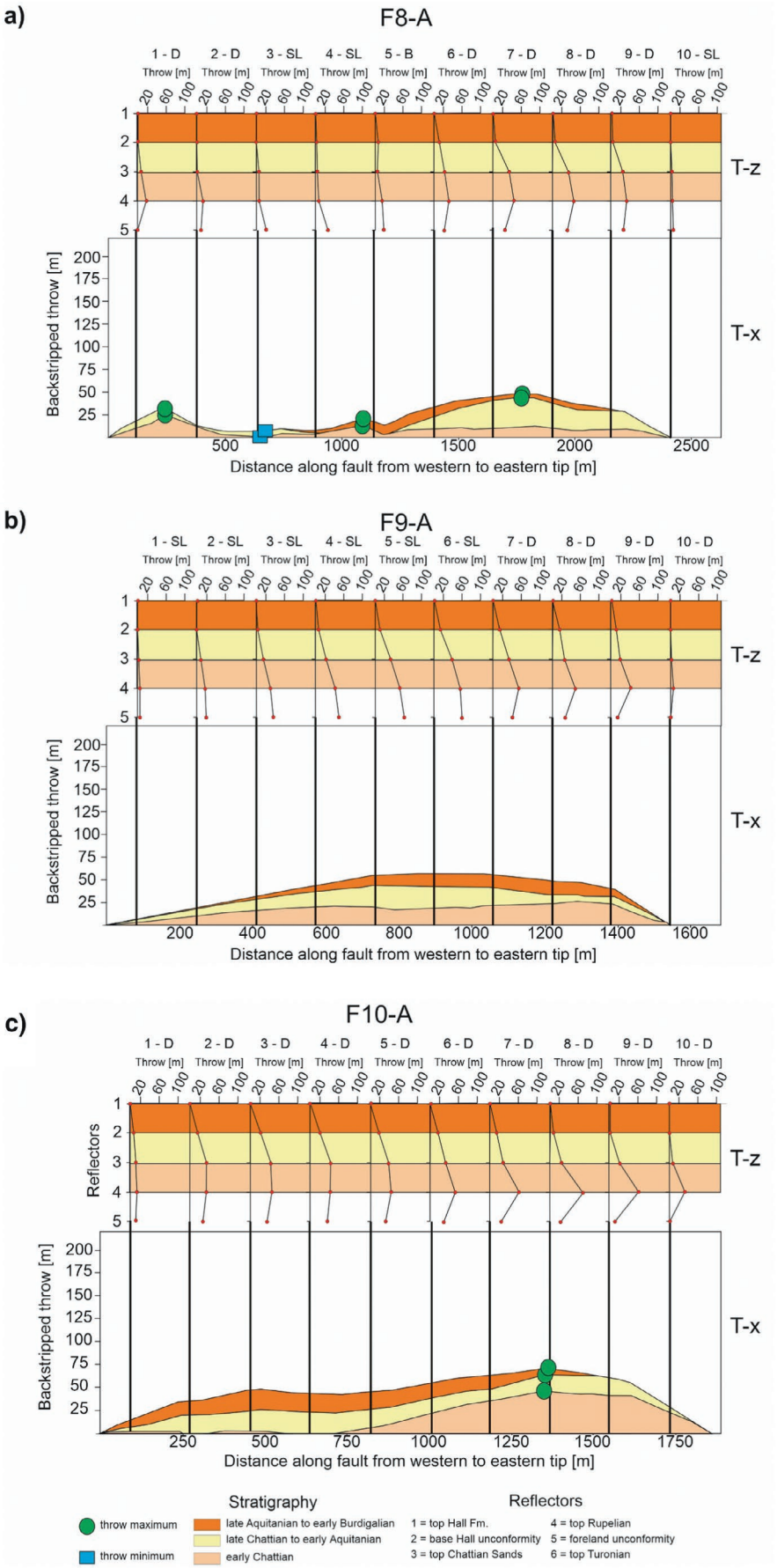

FIGURE A4 | T-x profile with 10 T-z profiles along the length of Faults (a) F8-A, (b) F9-A and (c) F10-A.

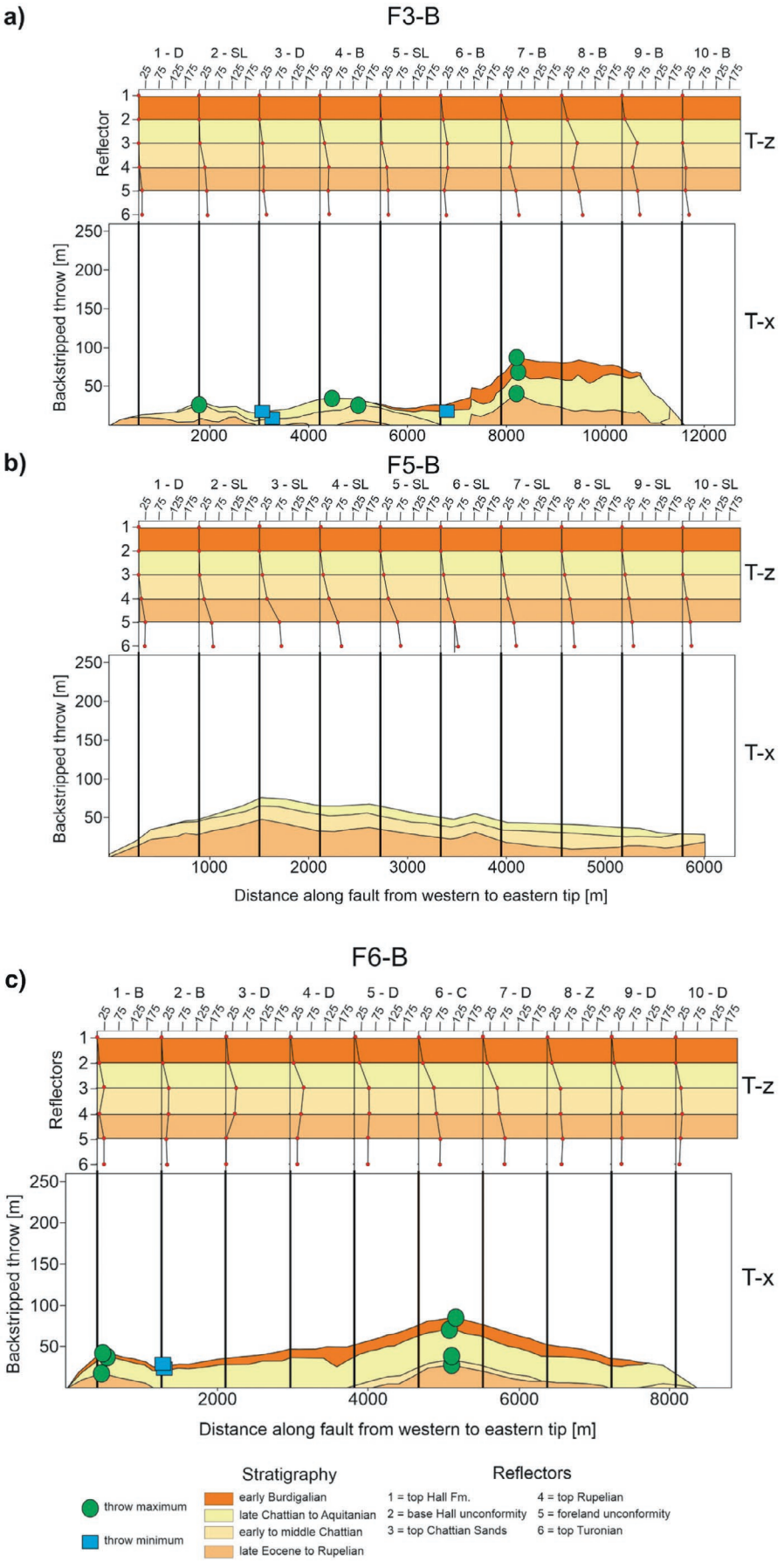

FIGURE A5 | T-x profile with 10 T-z profiles along the length of faults. (a) F3-B, (b) F5-B and (c) F6-B.

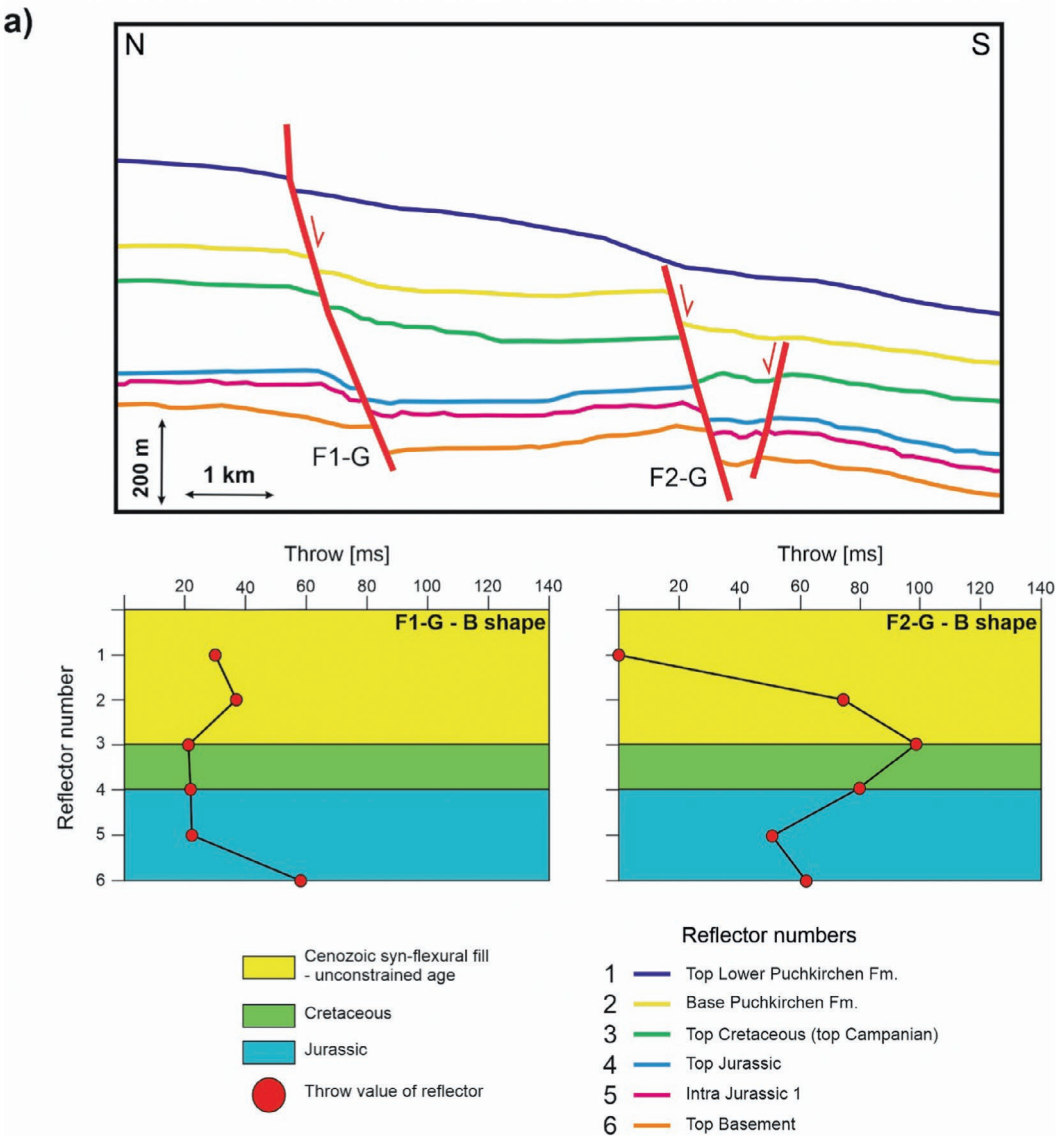

FIGURE A6 | (a) T-z profiles from two normal faults in the Austrian Molasse that cut the Cenozoic syn-flexural stratigraphy, based on seismic data in the Austrian Molasse (Gross et al. 2015, their figure 8). One extra reflector is interpreted within the Jurassic stratigraphy. T-z profiles indicate dip linkage of a lower segment with a Jurassic origin with upper segments that nucleated within the Cenozoic syn-flexural stratigraphy and at the foreland unconformity at the onset of flexural subsidence (F1-G and F2-G, respectively). (b) Interpretation of reflectors and syn-flexural normal faults in the Austrian Molasse (Masalimova et al. 2015, their figure 14). All T-z profiles have D-shapes, indicating isolated nucleation. For F1-MA, this section of the fault represents a Mesozoic fault that was reactivated during Cenozoic flexure. On the other hand, the T-z profiles from faults F2-MA and F3-MA have throw distributions suggestive of isolated nucleation at the foreland unconformity, subsequently propagating up- and downward. Therefore, it is likely these sections of the respective faults nucleated at the top of the Mesozoic basement at the onset of flexure as we observe in the German Molasse.